



Cite this: *Chem. Soc. Rev.*, 2023, **52**, 1672

## Emerging ultrasmall luminescent nanoprobe for *in vivo* bioimaging

Shihua Li,<sup>ab</sup> Jing Wei,<sup>bc</sup> Qiaofeng Yao,<sup>ce</sup> Xiaorong Song,<sup>\*bd</sup> Jianping Xie<sup>id \*ce</sup> and Huanghao Yang<sup>id \*abd</sup>

Photoluminescence (PL) imaging has become a fundamental tool in disease diagnosis, therapeutic evaluation, and surgical navigation applications. However, it remains a big challenge to engineer nanoprobe for high-efficiency *in vivo* imaging and clinical translation. Recent years have witnessed increasing research efforts devoted into engineering sub-10 nm ultrasmall nanoprobe for *in vivo* PL imaging, which offer the advantages of efficient body clearance, desired clinical translation potential, and high imaging signal-to-noise ratio. In this review, we present a comprehensive summary and contrastive discussion of emerging ultrasmall luminescent nanoprobe towards *in vivo* PL bioimaging of diseases. We first summarize size-dependent nano-bio interactions and imaging features, illustrating the unique attributes and advantages/disadvantages of ultrasmall nanoprobe differentiating them from molecular and large-sized probe. We also discuss general design methodologies and PL properties of emerging ultrasmall luminescent nanoprobe, which are established based on quantum dots, metal nanoclusters, lanthanide-doped nanoparticles, and silicon nanoparticles. Then, recent advances of ultrasmall luminescent nanoprobe are highlighted by surveying their latest *in vivo* PL imaging applications. Finally, we discuss existing challenges in this exciting field and propose some strategies to improve *in vivo* PL bioimaging and further propel their clinical applications.

Received 30th August 2022

DOI: 10.1039/d2cs00497f

[rsc.li/chem-soc-rev](http://rsc.li/chem-soc-rev)

<sup>a</sup> Qingyuan Innovation Laboratory, 1# Xueyuan Road, Quanzhou, Fujian 362801, China

<sup>b</sup> MOE Key Laboratory for Analytical Science of Food Safety and Biology, College of Chemistry, Fuzhou University, Fuzhou, Fujian 350116, China.

E-mail: [xrsong@fzu.edu.cn](mailto:xrsong@fzu.edu.cn), [hhyang@fzu.edu.cn](mailto:hhyang@fzu.edu.cn)

<sup>c</sup> Department of Chemical and Biomolecular Engineering, National University of Singapore, 4 Engineering Drive 4, Singapore 117585, Singapore. E-mail: [chexiej@nus.edu.sg](mailto:chexiej@nus.edu.sg)

<sup>d</sup> Fujian Science & Technology Innovation Laboratory for Optoelectronic Information of China, Fuzhou, Fujian 350108, China

<sup>e</sup> Joint School of National University of Singapore and Tianjin University, International Campus of Tianjin University, Binhai New City, Fuzhou, Fujian 350207, China



**Shihua Li**

*Shihua Li received her PhD degree from the College of Chemistry of Fuzhou University (China) in 2019 under the direction of Prof. Huanghao Yang. She is currently a postdoctoral researcher in collaboration with Prof. Yang. Her research interests focus on engineering nanoprobe for biomedical applications such as bioimaging, drug delivery, and theranostics.*



**Xiaorong Song**

*Xiaorong Song is currently an associate professor at College of Chemistry, Fuzhou University (China). He received his PhD in 2017 from Fuzhou University, and continued his visiting scholar study in National University of Singapore (NUS) and postdoctoral research at Fujian Institute of Research on the Structure of Matter, Chinese Academy of Sciences (China). His research interests focus on luminescent nanomaterials and their biomedical applications, especially on luminescent nanoprobe based disease diagnosis and bioimaging.*



# 1. Introduction

Medical imaging that utilizes imaging scanners to collect *in vivo* information has greatly advanced the development of diagnosis and therapy of human diseases.<sup>1</sup> Among the current nondestructive imaging techniques, photoluminescence (PL) imaging is one of the most important imaging tools in scientific and clinical research, due to its high sensitivity and specificity, multiplexing analysis and real-time dynamic imaging abilities.<sup>2,3</sup> As a result, PL imaging is promising for *in vivo* imaging, which enables the sensitive visualization of targets' concentration, activity, and other parameters as well as the diverse pathophysiological processes in the living body.<sup>4–6</sup>

Note that luminescent probes are used in PL imaging and ideally can generate sensitive and stable PL signals upon the specific recognition of certain analytes.<sup>7</sup> Organic fluorophores and fluorescent proteins have been widely applied in the design of luminescent probes. However, such conventional probes may face some problems, such as poor physicochemical stability and limited targeting efficacy to biomolecules and tissues.<sup>8,9</sup> Currently, luminescent nanoparticles (NPs) have aroused considerable attention in PL imaging because of their enhanced physicochemical stability and customizable surface and optical properties for multifunctional bioimaging.<sup>10–12</sup> Despite the exciting advances, *in vivo* PL imaging still encounters many issues including limited tissue penetration depth, interference of background PL and nonspecific tissue accumulation, and *in vivo* toxicity concern of luminescent nanoprobles. Therefore, it remains a challenge to establish sensitive and specific PL bioimaging platforms for *in vivo* clinical applications.<sup>13</sup>

With the considerable development of synthesis technologies of nanomaterials, sub-10 nm (the size refers to hard size determined using an electron microscope such as a transmission electron microscope) ultrasmall nanoprobles have attracted increasing attention in biological imaging applications (Fig. 1).<sup>14,15</sup> This is because ultrasmall nanoprobles generally

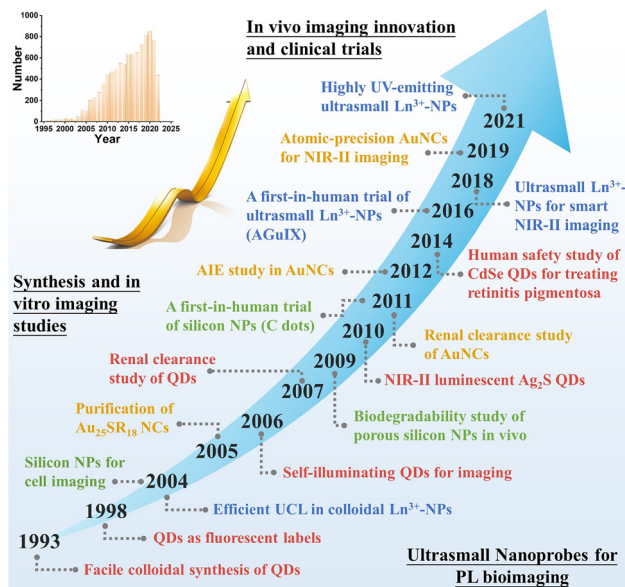


Fig. 1 Timeline of some significant events in the synthesis, bioimaging, and clinical trials of ultrasmall NPs. Inset: Count of paper result by searching "(ultrasmall OR quantum dot OR nanocluster) AND imaging" in Pubmed (obtained on July 27, 2022).

have a much weaker accumulation in the reticuloendothelial systems (RES) as compared to large-sized NPs, thus efficiently decreasing the background PL in major organs and enhancing the signal-to-noise ratio as well.<sup>16–19</sup> Besides, it is feasible to utilize ultrasmall nanoprobles for labelling and tracking *in vivo* targets without notably affecting their inherent transport traits in the living body. Moreover, ultrasmall nanoprobles can enable some unique *in vivo* bioapplications, such as PL imaging of kidney dysfunction and dual-modal *in vivo* PL imaging and *in vitro* urinalysis, which cannot be performed by large-sized nanoprobles.<sup>20–23</sup> Of note, the aforementioned hard size cannot offer dispersion information of NPs in suspension, thus necessitating the determination of hydrodynamic (HD) size by other



Jianping Xie

Jianping Xie is currently a Dean's Chair Associate Professor in the Department of Chemical & Biomolecular Engineering, National University of Singapore (NUS). He received his BS and MS degrees in Chemical Engineering from Tsinghua University (China), and his PhD from the Singapore-MIT Alliance (SMA) program. His group is known for the work on engineering water-soluble metal nanoclusters for biomedical and catalytic applications. Dr Xie is a Fellow of the Royal Society of Chemistry (FRSC).



Huanghao Yang

Huanghao Yang received his PhD from Xiamen University in 2002 and was engaged in postdoctoral research in Hong Kong University of Science and Technology (2002–2004). He joined Fuzhou University in 2008. He has been supported by National Science Foundation for Distinguished Young Scholars of China (2011) and the National Award for the Chang Jiang Scholar Program (2012). His research interests mostly focus on X-ray imaging, analytical chemistry, chemical biology, and nanomedicine. Prof. Yang is a Fellow of the Royal Society of Chemistry.



techniques such as dynamic light scattering (DLS). The HD size takes surface ligands and solvent into account and can sometimes affect the biological behaviors of NPs (*e.g.*, cell uptake, *in vivo* circulation and elimination, *etc.*).<sup>24</sup> For example, the common prerequisite to allow the renal clearance of NPs is to have HD size approaching (or lower than) the glomerular filtration threshold value ( $\sim 5\text{--}10$  nm). Ultrasmall nanoprobess with HD sizes in this range exhibit efficient renal clearance and low toxicity *in vivo*, promising future *in vivo* bioapplications.<sup>17,25</sup> Recently, several ultrasmall luminescent nanomaterials have been tailored for *in vivo* PL imaging, such as quantum dots (QDs), metal nanoclusters (NCs), lanthanide-doped NPs, and silicon NPs.<sup>26–32</sup> The developed ultrasmall nanoprobess have been implemented to analyze *in vivo* diseases – especially cancer-associated hallmarks, such as ions, small molecules, nucleic acids, proteins and enzymes. As such, it is anticipated that the ultrasmall luminescent nanoprobess will serve as potent PL imaging tools and provide a solution to *in vivo* imaging.<sup>33–35</sup> We should note that some specific challenges may also arise in the design and *in vivo* application of ultrasmall nanoprobess such as insufficient tumor targeting efficacy.

In this review, we provide a comprehensive summary of emerging ultrasmall luminescent nanoprobess towards PL imaging of diseases *in vivo*. Note that there is still a lack of systematic and contrastive discussion on the design and application principles of the emerging ultrasmall luminescent nanoprobess. We first summarize the size-dependent nano-bio interactions to understand the biodistribution, targeting, clearance, and toxicity of NPs. The unique advantages and

significant roles of ultrasmall nanoprobess in PL bioimaging *in vivo* are discussed, in comparison with traditional molecular and large-sized probes. We then detail the basic attributes, rational design methodologies, and *in vivo* PL imaging applications of four important kinds of ultrasmall luminescent inorganic nanoprobess, including QDs, metal NCs, lanthanide-doped NPs, and silicon (and silica) NPs (as illustrated in Fig. 2). Finally, we highlight the current challenges in this field, and propose potential strategies to improve *in vivo* PL imaging and propel clinical applications. We believe that this review may offer insights into *in vivo* PL bioimaging and propel future clinical translation of ultrasmall luminescent nanoprobess.

## 2. Size-dependent nano-bio interactions

Currently, different kinds of nanoagents have emerged in biological applications and in parallel their performances have been shown to be associated with their size, structure, and surface properties.<sup>36–38</sup> Due to these facts, it is important to understand nano-bio interactions prior to biological application studies. We here focus on summarizing and discussing material size effects on nano-bio interactions, including size-dependent *in vitro* cell uptake, biodistribution, and toxicity issues (Fig. 3).

### 2.1 Size-dependent *in vitro* cell uptake efficacy

Efficient cell uptake of NPs is a prerequisite for exerting desired biological imaging and therapy functions. Significantly, nanoagents

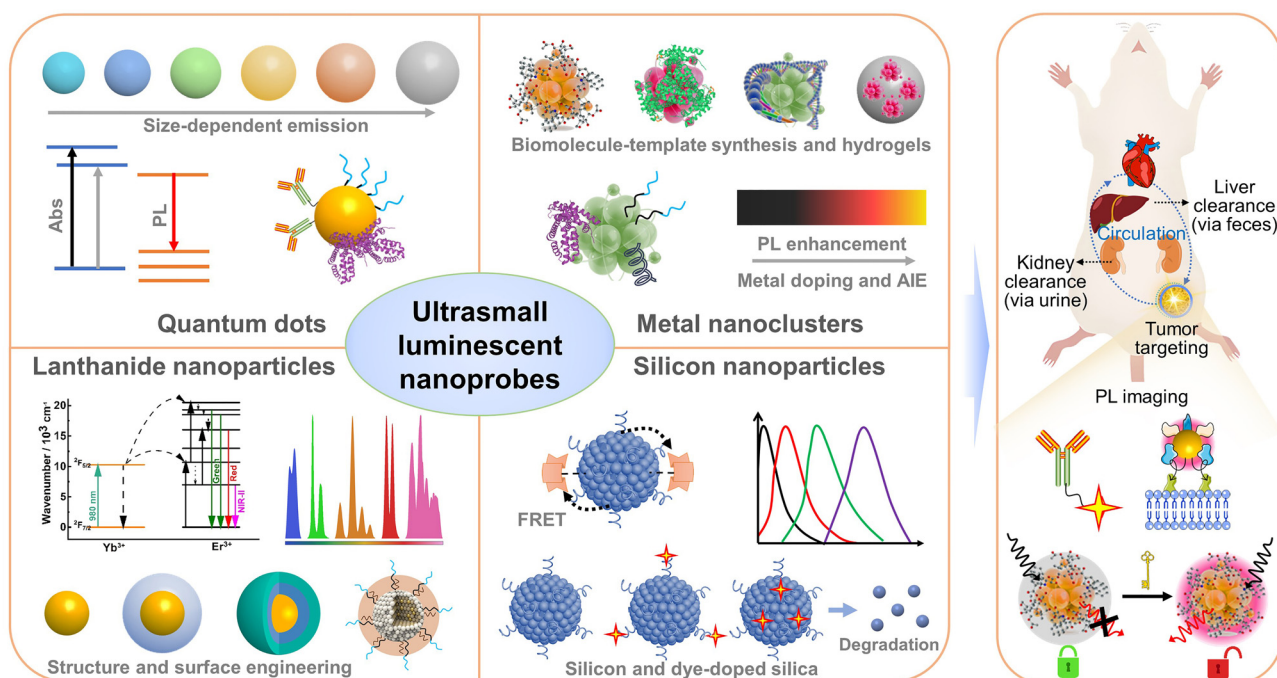


**Fig. 2** Schematic illustration of the design of ultrasmall luminescent nanoprobess and their clearance and bioimaging in mice. The synthesis and material structures, key luminescence properties, and surface engineering strategies of these ultrasmall luminescent nanoprobess are shown. After administration in the body, these ultrasmall nanoprobess can possibly be excreted *via* liver clearance and/or kidney clearance pathways. They can be implemented for diverse bioimaging, such as molecular labeling and tracking, analyte-activated imaging, and cell/tissue-targeted imaging.



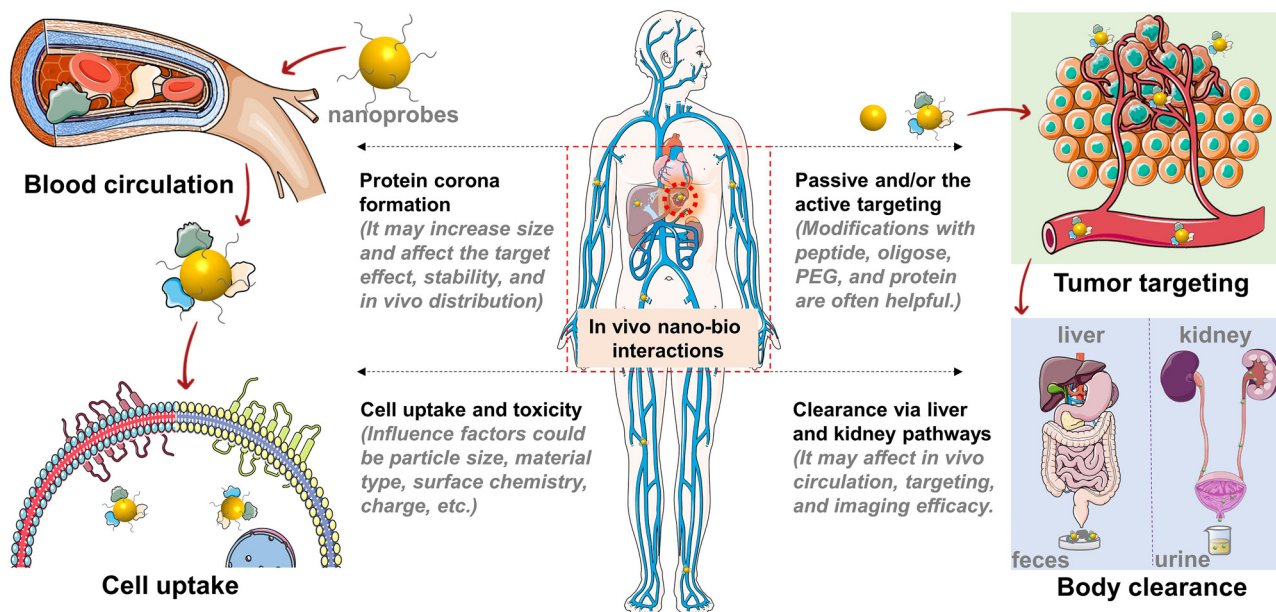


**Fig. 3** Schematic illustration of nano-bio interactions that may influence the *in vivo* pharmacokinetics, cell uptake, tumor targeting, and body clearance of nanoprobosc. The formation of protein corona on NPs and its effect on cell uptake are also shown. Note that disease targeting and body clearance properties are two crucial factors determining the *in vivo* imaging performance and clinical translation potential of nanoprobosc. Pictures were adapted with permission from Servier Medical Art by Servier (<https://smart.servier.com/>), licensed under a Creative Commons Attribution 3.0 Unported License.

can enter into the cells *via* multiple endocytosis pathways, while most small molecules (<1 kDa) penetrate into cells *via* simple diffusion, and macromolecules may have low endocytosis efficiency, with the exception of those showing strong binding to the receptors and/or cell membrane such as folate, transferrin, cell penetrating peptides, and so on.<sup>39–41</sup> This has also inspired the use of NPs for delivering cargos (such as drugs, nucleic acids, proteins, *etc.*) into cells.<sup>37</sup> However, it is difficult to achieve specific uptake of NPs by certain cell types due to their strong nonspecific adhesion and binding to the cell membrane.<sup>37</sup> Functionalization of targeting agents is a popular strategy to impart specific cellular uptake and subcellular organelle targeting abilities to NPs.<sup>42</sup> One should note that cell uptake is not always wanted, as in the case of cell membrane labeling.<sup>43–45</sup> In this context, conferring NPs with controllable uptake efficiency and intracellular location is one of the important objectives.

In the past few years, impressive efforts have been dedicated to understanding the effects of nanoparticle size on cell uptake, showing a vital role in the uptake pathway and efficacy of NPs. For example, Chan *et al.* found that herceptin conjugated gold NPs of hard size ranging from 2 to 100 nm showed a size-dependent internalization and the maximal cell uptake was observed in the 25–50 nm NPs.<sup>46</sup> In the case of mesoporous silica NPs (30–280 nm, hard size), Mou *et al.* also revealed the highest cell uptake occurring in the 50 nm NPs.<sup>47</sup> Note that the binding between the ligands of NPs and the receptors on the cell membrane can decrease Gibbs free energy, and result in membrane wrapping around the NPs.<sup>48</sup> The membrane-wrapping process is likely acceptable to describe the size-dependent uptake behaviors.<sup>49</sup> In this model, large-sized NPs

have more ligand-to-receptor interaction per particle than that in the small NPs, thus exhibiting higher cell uptake efficacy. However, the cell membrane may have receptor shortage and be unable to bind many NPs of >50 nm (hard size). The optimal size of NPs for cell uptake is determined as 30–50 nm.<sup>50</sup> In fact, there are currently some available methods to quantify the ligand number and density on NPs, which may provide further understanding on the size effect on cell uptake.<sup>51–53</sup> Cell uptake of ultrasml NPs has also been preliminarily studied. For instance, Liang *et al.* prepared tiopronin-coated Au NPs with hard sizes of 2–15 nm, and found size-dependent cell uptake efficacy in MCF-7 cells. Especially, Au NPs of 2 nm showed a higher cell uptake than 6 nm and 15 nm NPs.<sup>54</sup> Inconsistent with the results, the cell uptake efficacy of cationic Au NPs was found to be elevated with increasing hard size from 2, 4, to 6 nm, contrary to the results obtained with both anionic and zwitterionic counterparts.<sup>55,56</sup> This suggests that it is hard to obtain consistent trends of the size effect on cell uptake in different kinds of NPs.

Moreover, apart from size, cell uptake of NPs is also affected by other key factors such as surface chemistry, elasticity, and material shape.<sup>55,57–59</sup> Even for one particular factor, its effect on cell uptake should be evaluated case by case, similar to the aforementioned size effect on different materials. For instance, tuning elasticity has shown opposite effects on the cell uptake of silica nanocapsules and alginate-encapsulating liposomes.<sup>60,61</sup> Interestingly, at a certain particle size, it is possible to control cell uptake by tuning surface chemistry, in which surface ligands can be engineered to possess diverse properties such as density (or surface coverage), hydrophobicity, charge, and targeting motif.<sup>62–65</sup>



Therefore, cell uptake can be affected by size effect but is dominated by the combined effect of multiple factors.

## 2.2 Size-dependent protein corona and *in vivo* targeting

In order to understand the size effects on cell uptake efficacy, and *in vivo* biodistribution and targeting, the protein corona formation on NPs has attracted much research interest. The interplay between biological proteins and NPs is one of the decisive factors in the cell uptake process and *in vivo* pharmacokinetics.<sup>36,66</sup> When NPs are dispersed in the biological environment, serum proteins can dynamically adsorb on NPs, forming the so-called protein corona.<sup>67–70</sup> The protein corona can seriously affect the physicochemical properties, *in vitro* cell uptake, and *in vivo* fate of the NPs. For example, protein corona can facilitate or inhibit the binding of NPs to receptors on the cell membrane, thus affecting the cell–NP interactions.<sup>71,72</sup> The active targeting efficacy of functionalized NPs *in vivo* could be decreased due to the protein corona-induced rapid clearance and the shielding of surface targeting ligands.<sup>73,74</sup> Interestingly, recent studies showed that protein corona can also be beneficial for improving blood circulation and targeting by recruiting specific proteins.<sup>75–77</sup> Increasing the size of NPs has generally led to the increase of the binding constant and amount of proteins on NPs. Compared to large-sized NPs, ultrasmall NPs have smaller surface areas and permit the formation of only a thin-layer protein corona.<sup>78–81</sup> Such a reduced degree of serum protein coverage may retain the targeting capability of surface ligands and antibodies on NPs to a great extent. Even so, a deeper understanding of the protein corona of ultrasmall NPs is needed *via* experimental and theoretical studies.<sup>70,82</sup>

In comparison with molecules, NPs show significantly prolonged blood circulation and tissue targeting capability.<sup>58,83–85</sup> Particularly, NPs can exhibit passive targeting *via* the enhanced permeability and retention (EPR) effect and active targeting for enhanced accumulation in tumors.<sup>86</sup> However, clinical studies have shown that the EPR effect may not improve the accumulation of nanosized agents in human solid tumors, despite the success in preclinical animal models.<sup>87,88</sup> In addition, NPs are often prone to be sequestered by the RES (*e.g.*, liver, spleen, and bone marrow) after intravenous injection into animals. Similar to *in vitro* cell uptake, the particle size affects *in vivo* circulation, targeting and tissue penetration.<sup>58,89</sup> For example, larger NPs with a HD size of 20–100 nm often have improved pharmacokinetics and tumor targeting, but show limited tumor penetration ability and serious nonspecific accumulation in the RES, while smaller NPs (<10 nm) often show lower uptake in the RES and enhanced tissue penetration but a possible fast blood clearance. Besides, NPs of >200 nm tend to be accumulated in the spleen.

## 2.3 Size-dependent general toxicity and clearance pathway

Due to the exposure of main organs and tissues to NPs, it is of importance to guarantee low toxicity of NPs.<sup>90,91</sup> Owing to the high specific surface area, NPs have higher biological and chemical reactivity in comparison with bulk materials, resulting in potential toxicity concern.<sup>92</sup> One of the main

toxicity mechanisms of NPs is the formation of reactive oxygen species (ROS), which cause cell damage by the oxidation of intracellular substances, such as proteins, nucleic acids, and lipids.<sup>93</sup> This toxicity effect is likely dependent on the type and concentration of nanomaterials. Besides, nanotoxicity is also associated with the complex interplay between NPs and biomolecules (proteins and enzymes).<sup>94</sup> For example, the leaching of metal ions from metal-containing NPs might cause serious cytotoxicity and neurotoxicity. In this case, smaller NPs may have a faster ion release rate than larger NPs and induce higher cytotoxicity.<sup>95</sup> With the advance in nanomaterial engineering, the nanotoxicity of NPs can be modulated, and nanotoxicity has also been transformed into an effective therapeutic strategy for tumors (*e.g.*, selective ROS generation in cancer cells).<sup>96</sup> After administration in animals, *in vivo* toxicity is highly associated with the retention time of NPs in organs and tissues.

Nowadays, liver excretion (*via* feces) and renal clearance (*via* urine) are acknowledged as the two main pathways for the body clearance of NPs.<sup>97–100</sup> In contrast to liver clearance, renal clearance typically has a higher clearance efficiency (>50%) within a shorter period (*e.g.*, 12 h). To allow efficient body excretion *via* the renal clearance pathway, NPs usually should have HD sizes near or less than the glomerular filtration threshold. In addition, the size cut-off for renal clearance is also dependent on nanoparticle type (*e.g.*, hard or soft materials) and surface properties (*e.g.*, shape, hydrophobicity, and charge).<sup>101</sup> For example, several kinds of NPs with a HD size of ~10 nm were also found to be clearable by the kidney.<sup>102,103</sup> For NPs within the 2–6 nm range (HD size), smaller NPs are found to be cleared faster than the larger NPs, which could be due to their weaker interactions with the glomerular basement membrane.<sup>101</sup> As such, designing ultrasmall NPs with high renal clearance capability offers a promising solution to decrease long-term *in vivo* toxicity. This also inspires further exploration of smart large-sized NPs (that show specific degradation or disassembly into renal clearable molecules and ultrasmall NPs) for *in vivo* imaging application.<sup>104,105</sup>

## 3. Ultrasmall nanoprobe versus molecular and large-sized probes

The development of nanophotonics and nanomaterials has triggered the expansion of luminescent nanoprobe for diverse bioapplications. Unlike molecular probes, the surface chemistry of nanoprobe can be finely tailored to fulfill imaging purposes.<sup>106,107</sup> Nanoprobe are also able to solve the undesirable stability and optical tuning dilemmas in molecular probes, allowing multiplex imaging of targets.<sup>108</sup> Targeting units such as peptides, proteins, and small molecules can be attached to nanoprobe *via* several available bioconjugation methods.<sup>109</sup> This endows nanoprobe with passive and/or active targeting capability in tumors. Due to the specific size regime, ultrasmall nanoprobe fill the gap between molecular and large-sized probes, and sometimes provide a solution to the practical problems in disease targeting.



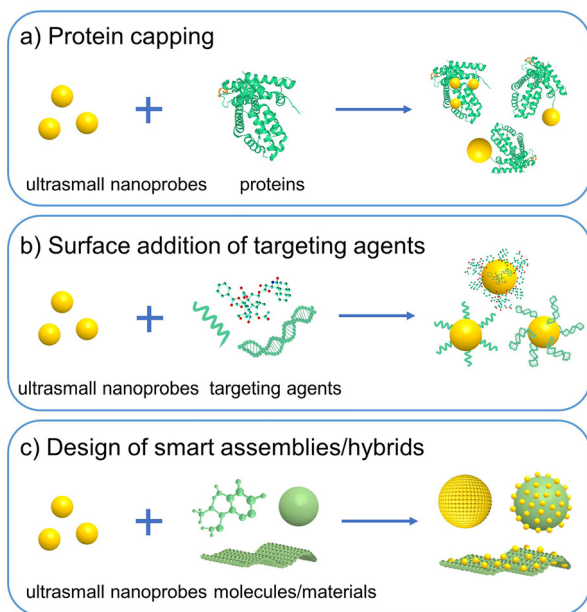


Fig. 4 Strategies to improve the *in vivo* tumor targeting efficacy of ultrasmall nanoparticles. (a) Protein capping on NPs via *in situ* synthesis or post-synthesis modification. (b) Surface functionalization with aptamers, peptides, ligands, and antibodies. (c) Designing ultrasmall NP-based smart assemblies and hybrids.

Even so, ultrasmall nanoparticles may have relatively low uptake in tumors than large-sized NPs due to their molecule-like renal clearance and fast blood clearance.<sup>21,110,111</sup> Impressively, some strategies have been presented to augment the tumor accumulation efficacy of ultrasmall nanoparticles.<sup>112–115</sup> For example, metal NPs can be synthesized *in situ* on template proteins (e.g., albumin), which may allow enhanced blood circulation and tumor accumulation effects than small-ligand-capped counterparts (Fig. 4a).<sup>116,117</sup> Functionalization of targeting agents (e.g., peptides, antibodies, and aptamers) may also be achievable (Fig. 4b); however, it is a big challenge to functionalize these targeting agents on ultrasmall NPs and maintain their renal clearance property. Currently, there are only a few successful examples such as those based on leveraging small antibodies and antibody fragments (with a molecular weight below  $\sim 40$  kDa).<sup>118,119</sup> Ultrasmall Au NCs and QDs could also self-assemble into large assemblies or integrate with other materials to form hybrids for increasing accumulation efficacy in the tumor and other desired sites (Fig. 4c).<sup>100,120,121</sup> This direction may be helpful to design smart assemblies for tumor-specific imaging and therapy application, which however is still in its infancy. Besides, the resultant assemblies may have increased nonspecific organ accumulation and different body clearance pathways.

Because of low unspecific accumulation in major organs, superior *in vivo* imaging quality with high signal-to-noise ratio can sometimes be realized by using ultrasmall nanoparticles.<sup>12,122</sup> More importantly, ultrasmall nanoparticles may feature a wider scope of *in vivo* imaging applications than the molecular and large-sized probes. For example, ultrasmall nanoparticles permit

some exclusive biological applications, such as *in vivo* PL bioimaging of kidney dysfunction and bladder-related diseases, and *in vivo* PL tracking of labeled proteins.<sup>123–125</sup> In addition, designing nanoprobes that feature target-activated release of renal clearable ultrasmall NPs offers a new strategy to diagnose *in vivo* diseases by urinalysis.<sup>22,126</sup> Such a methodology has facilitated *in vitro* multiplex analysis of *in vivo* targets.

## 4. Ultrasmall luminescent nanoprobes and *in vivo* bioimaging

As discussed above, ultrasmall luminescent nanoprobes offer new imaging tools for *in vivo* bioimaging applications. Currently, several important kinds of ultrasmall inorganic luminescent NPs have been engineered for *in vivo* PL bioimaging applications. In this section, we summarize the general features, design strategies, and *in vivo* imaging performance of ultrasmall luminescent nanoprobes based on QDs, metal NCs, lanthanide-doped NPs, and silicon NPs, respectively.

### 4.1 Quantum dots

**4.1.1 General features.** Semiconductor QDs are crucial luminescent tags that have been used in biological diagnosis and imaging since their successful colloidal synthesis.<sup>128,129</sup> In 1993, Bawendi and coworkers reported the facile production of nearly monodisperse QDs, inspiring the follow-up synthesis and biomedical application of QDs.<sup>130</sup> Due to the size approaching the bulk Bohr exciton radius (namely in the range of 2–10 nm), QDs show unique electrical and optical properties, especially nanocrystal size-dependent energy band gap.<sup>131,132</sup> Compared with fluorophores, QDs often exhibit better *in vivo* imaging performance, due to their narrow and tunable emissions covering from the visible to infrared regions, robust photostability, large absorbance coefficients, and high quantum yields.<sup>133</sup> For instance, the PL wavelength of QDs can be readily tuned by controlling particle sizes, compositions, and internal structures.<sup>134,135</sup> Currently, researchers have developed a number of approaches to synthesize QDs, including bottom-up methods (e.g., wet chemistry, pyrolysis, hydrothermal methods, etc.) and top-down methods (e.g., electrochemical etching, laser ablation, etc.).<sup>136,137</sup> Besides, surface functionalization of QDs can be conducted by diverse modification strategies, such as ligand exchange, amphiphilic polymer coating and silica coating.<sup>133,138</sup> Such attributes make QDs an important label for molecular PL imaging *in vivo*.

Typically, metal chalcogenide QDs are composed of elements from Group II–VI (e.g., CdSe, CdTe, HgTe) and IV–VI (e.g., PbS, PbSe). The earlier works based on these QDs have brought them to the forefront in biomedical imaging. However, heavy metal elements, such as Cd, Hg, and Pb, are rather toxic to cells. Besides, although it is currently a routine to synthesize QDs with near-infrared (NIR) PL (700–900 nm), their excitation wavelength still lies in the visible region ( $< 500$  nm), which hinders *in vivo* practical application. To circumvent such issues, the past years have witnessed the rapid development



of core-shell QDs with an inert shell (*e.g.*, ZnS) and low-toxicity QDs without heavy metals, including Group III-V (*e.g.*, InP, InAs), I-VI (*e.g.*, Ag<sub>2</sub>S, Ag<sub>2</sub>Se),<sup>139</sup> and I-III-VI (*e.g.*, CuInSe, AgInS<sub>2</sub>). These QDs may have improved *in vivo* long-term biostability and also extend emission wavelength into the second NIR region (NIR-II, 1000–1700 nm). Over the past few decades, the *in vitro* and *in vivo* toxicity effects of QDs have attracted much research, as summarized in several nice reviews.<sup>140–142</sup> The toxicity of QDs is mostly caused by the release of metal ions and ROS formation, which are dependent on dosage, composition and surface chemistry properties. Generally, inert shell coating and biomolecule/PEG modifications could be beneficial for reducing the potential toxicity.<sup>143</sup>

**4.1.2 Biodistribution and body clearance.** The *in vivo* bio-distribution fate of QDs is largely dependent on the surface properties (*e.g.*, ligands, charges, and proteins) and particle size.<sup>145,146</sup> In 2007, Bawendi and Frangioni *et al.* studied the size and surface charge effects of QDs on their urinary excretion properties after intravenous injection.<sup>127</sup> The QDs were synthesized in an organic phase and coated with zwitterionic or neutral organic ligands to render water dispersibility. The authors found that QDs with a HD diameter of <5.5 nm were effectively cleared into the urine within a few hours (Fig. 5). This study provides a foundation for future exploitation of renal clearable nanoagents for biomedical application. However, the HD size of QDs may be increased (*e.g.*, >10 nm) after surface modification with polymers, proteins, and antibodies. These QD nanoproboscopes may be sequestered by the liver and encounter subsequent slow hepatic clearance *via* the feces.<sup>133,147</sup> For example, Wang *et al.* reported the encapsulation of Ag<sub>2</sub>S QDs in protein nanocages (PNC) and their further modification with

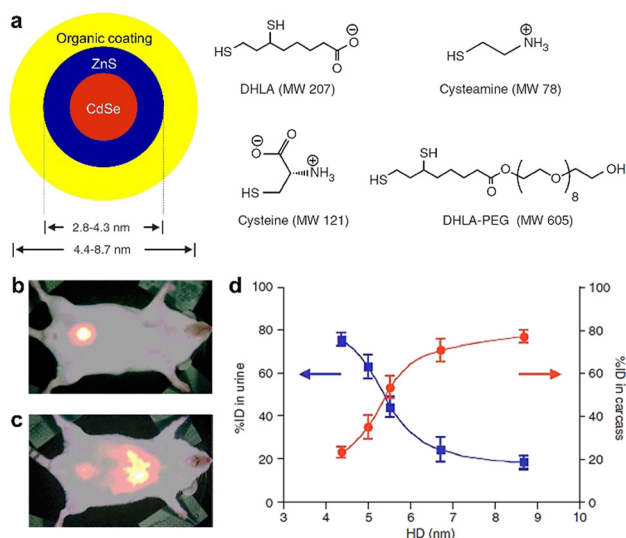


**Fig. 5** (a) Sketch map of the core-shell QDs and the chemical structure of the used ligands. (b and c) Overlay of the bright field images and gamma-ray images of mice at 4 h post intravenous injection of <sup>99m</sup>Tc-QD515 (4.36 nm, HD size) and <sup>99m</sup>Tc-QD574 (8.65 nm, HD size). (d) Urine excretion (blue curve) and carcass retention (red curve) of <sup>99m</sup>Tc-QDs with various HD diameters at 4 h after the injection. Adapted with permission.<sup>127</sup> Copyright 2007, Springer Nature.

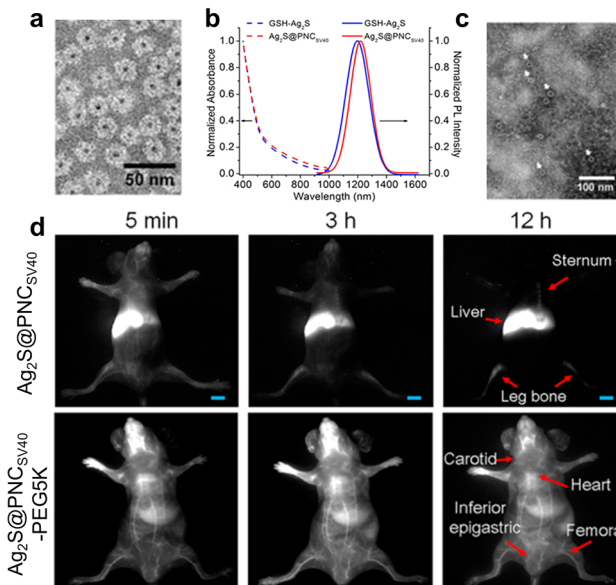


**Fig. 6** (a) Negatively stained TEM image of Ag<sub>2</sub>S-PNC. (b) Absorption and PL spectra of the synthesized nanoproboscopes. (c) TEM image of Ag<sub>2</sub>S-PNC after incubation with serum for 2 days. (d) *In vivo* real-time NIR-II tracking of Ag<sub>2</sub>S-PNC and PEGylated Ag<sub>2</sub>S-PNC after intravenous injection. Adapted with permission.<sup>144</sup> Copyright 2015, American Chemical Society.

polyethylene glycol (PEGylation), which both led to their major accumulation in the liver, but the blood circulation time was significantly prolonged after PEGylation (Fig. 6).<sup>144</sup> Dai *et al.* also found the size increase of the synthesized QDs from 6.9 nm (hard size) to 18.2 nm (HD size) after PEGylation. The resulting QDs enabled sensitive *in vivo* imaging of tumor and can be mainly excreted in 72 h *via* the biliary pathway (Fig. 7).<sup>148</sup> In addition, the biological stability of QDs should be considered to avoid potential toxicity of metal ions caused by decomposition.<sup>149</sup> Thereby, careful functionalization of QDs with suitable agents is necessary to impart body-clearable and disease-targeted imaging capabilities to QD nanoproboscopes for improving bioimaging efficacy.

**4.1.3 *In vivo* PL bioimaging.** To avoid the potential toxicity of heavy metal ions (*e.g.*, Cd, and Hg) in animals, toxic-metal-free QDs with outer ZnS shells are the ideal choices for bioimaging.<sup>131</sup> Importantly, the ZnS shell can also lower the toxicity of Cd/Pb-based QDs, as evidenced by the minimal *in vivo* toxicity of CdSe/Cds/ZnS and Pbs/Cds/ZnS QDs.<sup>150–152</sup> To bypass the possible toxicity of heavy metal ions, Pons *et al.* synthesized core-shell CuInS<sub>2</sub>/ZnS QDs with intense emissions centered at 800 nm and a high quantum yield (QY) of 20%, which retained bright fluorescence after dispersing in water and were applied to *in vivo* sensitive imaging of sentinel lymph nodes.<sup>153</sup> The QDs also had a better stability and lower *in vivo* acute toxicity in comparison with Cd-containing QDs. By contrast, CuInS<sub>2</sub> QDs were found to evoke serious *in vitro* and *in vivo* toxicity when there was no ZnS shell coating, corroborating the significance of the surface inert shell in reducing toxicity.<sup>154</sup> The QY of core-shell CuInS<sub>2</sub>/ZnS QDs can be further improved to 70–80% by using template and cation exchange



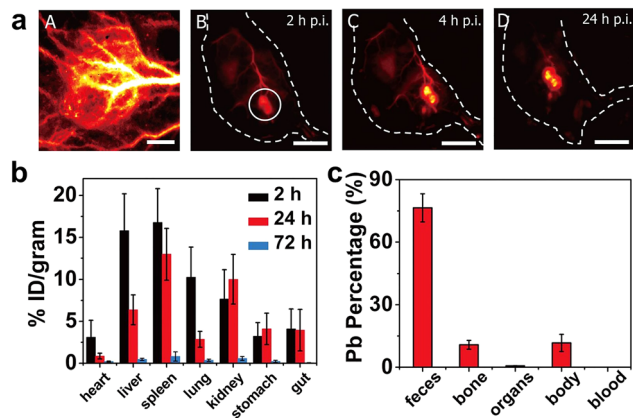


Fig. 7 (a) Time evolution of *in vivo* tumor imaging of PEGylated PbS/CdS QDs. (b) Biodistribution of QDs at different time after intravenous injection. (c) Excreted percentage of Pb in various parts of mice at 28 d post injection. Adapted with permission.<sup>148</sup> Copyright 2018, National Academy of Sciences.

synthesis methods.<sup>155,156</sup> Upon functionalizing QDs with targeting agents, like peptides, nucleic acids, and antibodies, cancer-targeted PL imaging was realized to visualize *in vivo* tumors.<sup>129,157,158</sup> For instance, Pang and colleagues doped Mn<sup>2+</sup> into Ag<sub>2</sub>Se QDs, conferring QDs with both NIR PL imaging and magnetic resonance imaging abilities.<sup>159</sup> The ultrasmall nanoprobe (HD, 4.3 nm) were encapsulated in the cell-derived microvesicles (MVs) for labeling, thereby enabling whole-body tracking of MVs *via* dual-modal imaging. Also, emission-tunable QDs allow multicolor and multiplex PL imaging by targeting different biomarkers.<sup>160,161</sup> In order to improve *in vivo* imaging specificity, QDs can be engineered with target-activatable linkers (*e.g.*, enzyme-responsive peptides) and energy acceptors (*e.g.*, dyes), thus enabling specific PL imaging of targets *via* modulating Förster resonance energy transfer between the QDs and acceptors. This strategy has been implemented to image cancer-associated markers, including proteases, ions (*e.g.*, H<sup>+</sup>, metal ions), small molecules (*e.g.*, reactive oxygen species), and nucleic acids (*e.g.*, mRNA, microRNA).<sup>162–165</sup> Interestingly, in 2006, Rao *et al.* introduced self-illuminating QD conjugates for *in vivo* multiplex imaging.<sup>166</sup> Through the bioluminescence resonance energy transfer between QDs and luciferase, the conjugates emitted bright PL for *in vivo* imaging with a high signal-to-background ratio. So far, the self-illuminating QD nanoprobe have been developed by several design strategies, providing multifunctional autofluorescence-free tools for *in vivo* imaging of diverse diseases.<sup>167–170</sup>

In comparison with PL imaging in the NIR-I region (700–900 nm), NIR-II imaging techniques have realized better imaging sensitivity and resolution in deep tissues, due to significantly reduced light scattering and tissue absorption as well as negligible background PL in such a spectral range. Currently there are several kinds of NIR-II QDs, mainly including PbS, Ag<sub>2</sub>S, InAs, and CuInS<sub>2</sub>.<sup>171–175</sup> In 2010, Wang *et al.* first reported the synthesis of monodisperse NIR-II Ag<sub>2</sub>S QDs with a hard size of 10 nm and PL emission at ~1058 nm.<sup>176</sup>

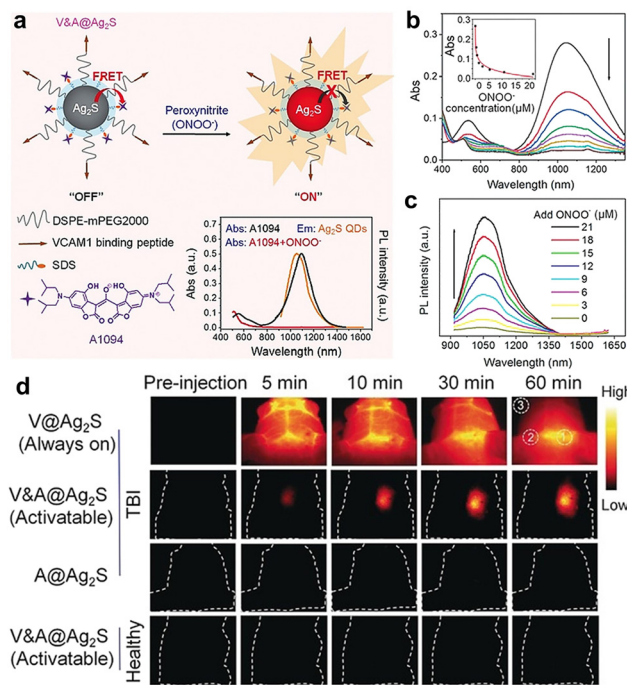


Fig. 8 (a) Schematic diagram of activatable Ag<sub>2</sub>S QD nanoprobe. (b and c) Absorbance and PL spectra of nanoprobe upon treatment with various concentrations of ONOO<sup>-</sup>. (d) *In vivo* imaging performance of nanoprobe in mice with brain vascular injury and control mice, respectively. Adapted with permission.<sup>177</sup> Copyright 2019, Wiley-VCH.

Wang *et al.* recently developed activatable NIR-II nanoprobe for real-time assessment of the early traumatic brain injury (Fig. 8).<sup>177</sup> Bruns *et al.* exploited the NIR-II-emitting InAs-based core-shell QDs with a QY up to 30%, and demonstrated multifunctional *in vivo* PL imaging applications, such as quantitative blood flow mapping in brain and tumor microvascular imaging in mice (Fig. 9).<sup>178</sup> Importantly, activatable NIR-II QD nanoprobe show high imaging sensitivity and specificity to targets of interest, and are increasingly explored for specific diagnosis of cancer and PL imaging-guided surgery.<sup>179,180</sup> Ultrasmall QDs will serve as promising imaging toolkits for *in vivo* bioimaging, but it may still not be easy to make such multifunctional QD nanoprobe renal clearable currently.

## 4.2 Metal nanoclusters

**4.2.1 General features.** Metal NCs, such as Au, Ag, Cu, and Pt NCs, are ultrasmall metal NPs that generally have core sizes below 2 nm.<sup>181,182</sup> Herein, we focus on Au NCs in view of their good physicochemical stability and low tissue toxicity. Due to the definitive atom number and molecular formulae, atomically precise metal NCs provide the missing links between the atoms and nanocrystals (> 3 nm).<sup>183,184</sup> Owing to the ultrasmall size approaching the Fermi wavelength of electrons, Au NCs show discrete electronic states and attractive optical absorption and PL properties. In particular, Au NCs usually feature tunable PL from UV to NIR regions, long lifetime ( $\mu$ s level), large Stokes shift (> 100 nm), and high photostability. Such attributes make Au NCs interesting ultrasmall luminescent nanoprobe for



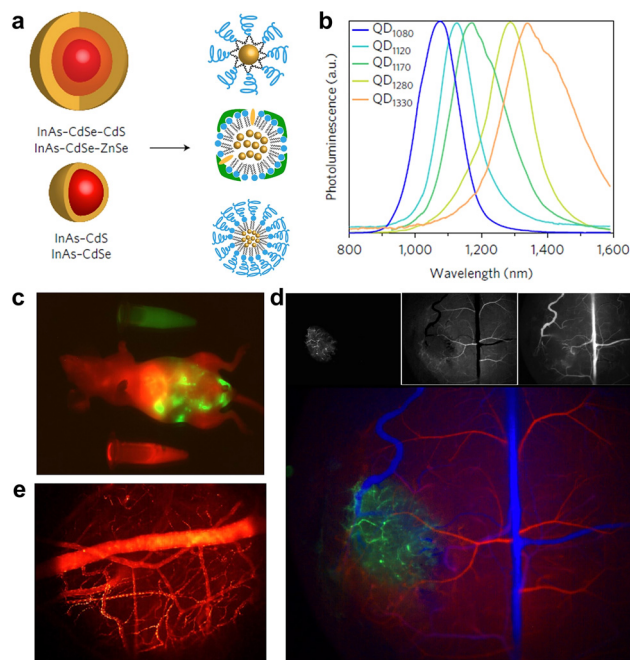


**Fig. 9** (a) Schematics of core-shell structures of the designed QDs and surface functionalization with phospholipid micelles (upper), lipoproteins (middle), and emulsified composite QDs (bottom). (b) PL spectra of the synthesized QDs. (c–e) Multicolor whole-body imaging, brain angiograph and blood flow mapping after intravenous injection of QDs, respectively. Adapted with permission.<sup>178</sup> Copyright 2017, Springer Nature.

biosensing and bioimaging.<sup>110,185,186</sup> Despite the general low toxicity, Au NCs also have toxicity concern caused by the induced ROS generation in cells and organs. Especially, protein-protected Au NCs have shown toxicity to liver, kidney, and spleen after long-term accumulation in organs, while no toxicity was observed in small-ligand-capped Au NCs.<sup>187,188</sup> Besides, a serious cytotoxicity of ultrasmall Au NPs (1 nm, hard size) capped with organic ligands was observed.<sup>189</sup> Therefore, the toxicity of Au NCs is highly related to surface ligands, which might dominate their interaction with cells/biomolecules and the *in vivo* clearance way.<sup>190</sup>

Typically, Au NCs are synthesized by reducing metal precursors in the presence of certain protective ligands, such as thiolates, polymers, proteins, and nucleic acids.<sup>191–193</sup> Apart from “bottom-up” synthesis strategies, Au NCs can also be obtained through the “top-down” etching strategy. Thiolate ligands are commonly used to synthesize water-soluble metal NCs.<sup>194</sup> In 2005, Tsukuda *et al.* synthesized and purified glutathione (GSH) capped Au NCs, and characterized the classical Au<sub>25</sub>(SG)<sub>18</sub> NCs by using high-resolution electrospray ionization mass spectrometry.<sup>195</sup> To prepare high-purity Au NCs, a “size focusing” method has been developed and proven effective for the synthesis of numerous NCs, such as Au<sub>25</sub>(SR)<sub>18</sub>,<sup>196</sup> Au<sub>38</sub>(SR)<sub>24</sub>,<sup>197</sup> and Au<sub>144</sub>(SR)<sub>60</sub> NCs,<sup>198</sup> which can be applied to versatile thiolate ligands.<sup>199</sup> By employing CO gas as a reducing agent, Xie’s group developed a facile way to synthesize a series of atomically precise Au NCs.<sup>200</sup> Interestingly, thiolate-capped Au NCs can further be modified for

diverse bioimaging and therapy applications *via* several strategies, such as ligand exchange/addition, protein functionalization, and the formation of hybrid nanomaterials.<sup>193</sup>

Compared with the organic fluorophores and aforementioned QDs, Au NCs (such as thiolate-protected Au NCs) have a relatively low QY (typically <10%).<sup>202,203</sup> Additionally, sometimes PL origins of Au NCs remain elusive, which could be due to the lack of enough precise structures and PL information of Au NCs. In order to improve the PL property of Au NCs, great efforts have been devoted into modulating the composition, structure and surface rigidity. For example, Zhu and coworkers introduced the silver doping strategy to dramatically augment the PL QY of Au<sub>25</sub> NCs by ~40%.<sup>204</sup> Lee *et al.* reported the distinct enhancement of Au<sub>22</sub>(SG)<sub>18</sub>’s QY by rigidifying the Au(I)-thiolate shell with surface bulky groups, and achieved a QY of ~60%.<sup>205</sup> Similar to the aggregation-induced emission (AIE) phenomenon in the organic AIE nanodots, Xie *et al.* observed the poor solvent-induced aggregation and large PL enhancement in the Au(I)-GSH complexes. Subsequent one-pot synthesis of Au NCs by aggregation of Au(I)-GSH complexes on the *in situ* generated Au(0) core resulted in a high QY of ~15%.<sup>206</sup> Xie *et al.* further conducted systematic spectroscopic investigations on a series of Au(I)-GSH complexes and the atomically precise GSH-Au NCs.<sup>207</sup> This study reveals the efficient modulation of the PL origins of Au NCs and their emission wavelengths (from the visible to NIR-II regions) by controlling the length of the surface Au(I)-thiolate motif, which provides new insights to control the emission wavelength and intensity of thiolate-protected Au NCs. Apart from the above strategies, Au NCs’ QY can also be enhanced by confinement and self-assembly approaches.<sup>208–211</sup>

**4.2.2 Molecule-like *in vivo* biodistribution property.** Unlike large-sized NPs, Au NCs with HD sizes of ~2 nm tend to be quickly cleared out from the body *via* kidney filtration, similarly to small molecules. In 2011, Zheng *et al.* first reported the high-efficiency renal clearance (>60%) of luminescent GSH-Au NCs within 24 h after intravenous injection (Fig. 10), while citrate and cysteine protected Au NCs were prone to be accumulated in the RES (especially liver and spleen).<sup>201</sup> This reveals a vital role of surface chemistry in dominating the biodistribution fate of Au NCs. Oppositely, molecule-like Au NCs possess a relatively short blood circulation time, which may invalidate the EPR effect for passive tumor targeting. Liu and Zheng found that PEGylation (with a molecular weight of ~1 kDa) was capable of endowing Au NCs with enhanced tumor targeting, prolonged blood circulation lifetime, and effective renal clearance, in contrast to GSH-Au NCs (Fig. 11).<sup>212</sup> Besides, Au NCs can be functionalized with additional agents (*e.g.*, folate, peptides, and antibodies) for active tumor targeting.<sup>186</sup> Interestingly, Zheng *et al.* found that GSH-mediated biotransformation in the liver can modulate the transport of NPs *in vivo*.<sup>213</sup> The indocyanine green (ICG)-modified Au<sub>25</sub> NCs were first transported to the liver and then transformed into renal clearable ICG and GSH-Au<sub>25</sub> for systemic blood circulation. This resulted in the enhanced tumor accumulation of ICG and GSH-Au<sub>25</sub> NCs, offering a strategy to tailor *in vivo* targeting and clearance of



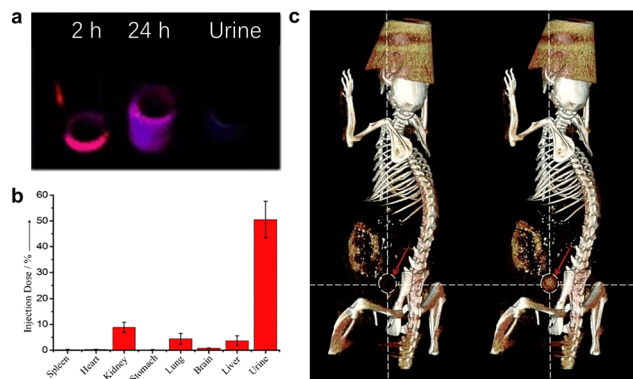


**Fig. 10** (a) Time-dependent PL images of urine samples post intravenous injection under UV excitation. (b) Biodistribution of GSH-Au NCs in mice at 24 h post injection. (c) X-ray computed tomography images of mice before (left) and after (right, 30 min) the injection of GSH-Au NCs. Adapted with permission.<sup>201</sup> Copyright 2011, Wiley-VCH.

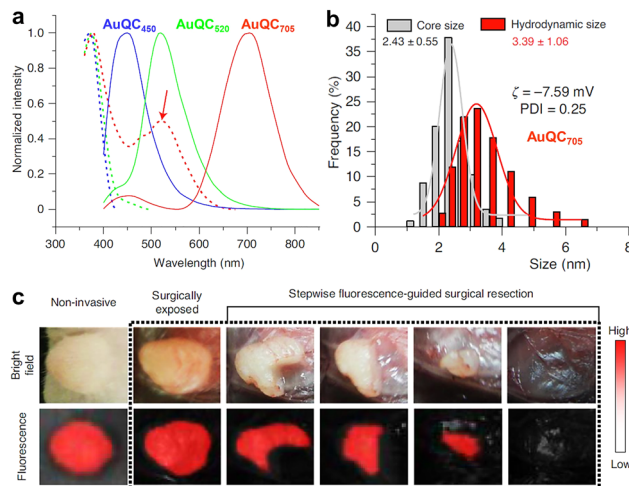


**Fig. 12** (a) Excitation (dotted lines) and emission (solid lines; excitation, 360 nm) spectra of emission-tunable Au NCs. (b) Core size, zeta potential, and HD diameter of the 705 nm-emitting Au NCs. (c) PL imaging guided intraoperative surgery of *in vivo* mouse tumors. Adapted with permission.<sup>217</sup> Copyright 2020, Springer Nature.

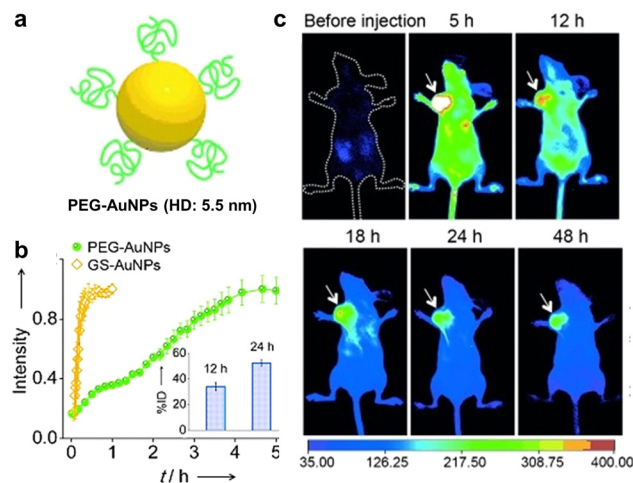


**Fig. 11** (a) Schematic illustration of PEG-Au NCs and HD size. (b) Renal clearance kinetics of PEG- and GS-Au NCs. Inset: PEG-Au NC contents in urine at 12 and 24 h post injection. (c) Time-dependent PL images of mice after injection (arrows indicate the tumor sites). Adapted with permission.<sup>212</sup> Copyright 2013, Wiley-VCH.

ultrasmall nanoprobe. It should be noticed that the core size, length of the ligand, surface charge and protein corona could also affect the biodistribution of Au NCs.<sup>21</sup> For *in vivo* applications, high-efficiency renal clearance of Au NCs can increase the signal-to-noise ratio in the targeted site after the elimination of off-target NCs.<sup>214</sup> Based on these findings, Au NCs could hold great clinic translation potential.<sup>22,101</sup>

**4.2.3 *In vivo* PL bioimaging.** In the bioimaging field, the unique advantage of Au NCs could be their low toxicity, rapid body clearance, and theranostic functions.<sup>215,216</sup> The favorable NIR-emitting Au NCs can be synthesized by directly using peptides and proteins as both capping and active targeting agents. For instance, Kircher and colleagues recently reported a series of emission-tunable Au NCs with HD sizes of ~2–6 nm that were protected by low molecular mass metalloprotein

alpha-lactalbumin ( $\alpha$ -LA).<sup>217</sup> The Au NCs showed a high tumor accumulation ability for effectively visualizing *in vivo* breast tumors and guiding the tumor resection process (Fig. 12). Besides, the  $\alpha$ -LA-capped Au NCs not only enabled dual-modal bioimaging by integrating X-ray computed tomography with magnetic resonance imaging, but also utilized cytotoxic  $\alpha$ -LA-oleic acid complexes for tumor theranostics.

Beyond always-on PL imaging, Au NCs can be assembled with other types of luminescent agents for turn-on or ratiometric imaging of analytes (*e.g.*, ROS).<sup>219–222</sup> Additionally, luminescent Au NCs with an efficient renal clearance feature can serve as imaging agents to noninvasively monitor the renal clearance kinetics and image kidney diseases.<sup>223,224</sup> To improve the *in vivo* targeting efficacy to tumors, it is required to tailor the pharmacokinetics and biodistribution of Au NCs, which could be achieved by surface modifications. For example, Liu *et al.* recently synthesized the charge-reversal luminescent Au NCs protected with thiolate PEG and small ligands, which had optimized pharmacokinetics and pH-regulated HD sizes and surface charges.<sup>218</sup> Such nanoprobe enabled high tumor targeting for the selective PL imaging of tiny metastatic tumors in the liver and lungs (Fig. 13). Importantly, Au NCs may retain the HD sizes below 6 nm even after further functionalization of some small-sized agents (*e.g.*, antibody, protein, PEG), while QDs with similar modifications may have overall sizes of >10 nm and couldn't be renal clearable.

In recent years, NIR-II PL has been observed in classical thiolate-protected Au<sub>25</sub> NCs, which provide better PL imaging contrast than the conventional NIR-I-emitting Au NCs.<sup>225,226</sup> The NIR-II PL was found to be enhanced by precise doping of metal ions (such as Zn<sup>2+</sup>), thus allowing for the sensitive imaging of brain blood flow dynamics and cancer metastasis.<sup>227</sup> By using cyclodextrin (CD) as the capping agent, we and colleagues recently synthesized CD-Au NCs with an intense



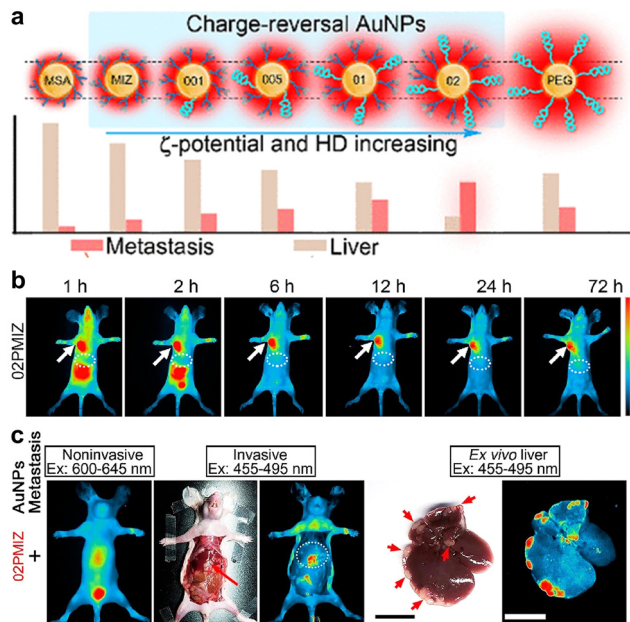


**Fig. 13** (a) Schematic of Au NCs with identical core sizes ( $\sim 1.7$  nm) and different modifications and HD sizes. (b) PL imaging of mice after injection of the optimized Au NCs. (c) Whole-body and ex vivo liver imaging of liver-metastasis-bearing mice at 24 h post injection (arrows show the liver and metastasis sites). Adapted with permission.<sup>218</sup> Copyright 2020, American Chemical Society.

emission at  $\sim 1050$  nm.<sup>125</sup> The NCs not only feature efficient renal clearance, but also enable robust protein/antibody labeling *via* the host-guest interaction for *in vivo* tracking and tumor-targeted PL imaging (Fig. 14). Also, Li *et al.* developed the ribonuclease-A capped Au NCs with bright NIR-II emissions for gastrointestinal tract imaging and intestinal tumor diagnosis, due to their outstanding photostability in the gastric environment.<sup>228</sup> By virtue of the high renal clearance efficiency and decreased potential toxicity, luminescent Au NCs are increasingly explored as ultrasmall nanoprobe and promise future clinical translation.<sup>229,230</sup>

### 4.3 Lanthanide-doped nanoparticles

**4.3.1 General features.** Lanthanides are the important 15 elements covering from lanthanum (atomic number 57) to lutetium (atomic number 71), which are considered as rare earth elements together with scandium and yttrium. Lanthanide ions ( $\text{Ln}^{3+}$ ) have the electron configuration of  $4f^n 5s^2 5p^6$  ( $n = 0-14$ ), and emit tunable emissions covering from UV, visible, to NIR regions originating from the  $4f-4f$  transitions.<sup>231-234</sup> When doped into suitable host crystalline lattices or coordinating with suitable ligands,  $\text{Ln}^{3+}$  have intense, narrow, tunable emissions with good photostability, because of the well-defined and ladder-like energy levels.<sup>235-238</sup> In addition, their  $4f$  orbitals are shielded by the filled  $5s$  and  $5p$  orbitals, providing stable and distinguishable spectroscopic signals for PL bioimaging in the biological environment.<sup>239,240</sup> Moreover,  $\text{Ln}^{3+}$  ions show long-lived luminescence and narrow band emissions, which enable time-resolved optical imaging and multiplex PL imaging.<sup>241,242</sup> In 2004,

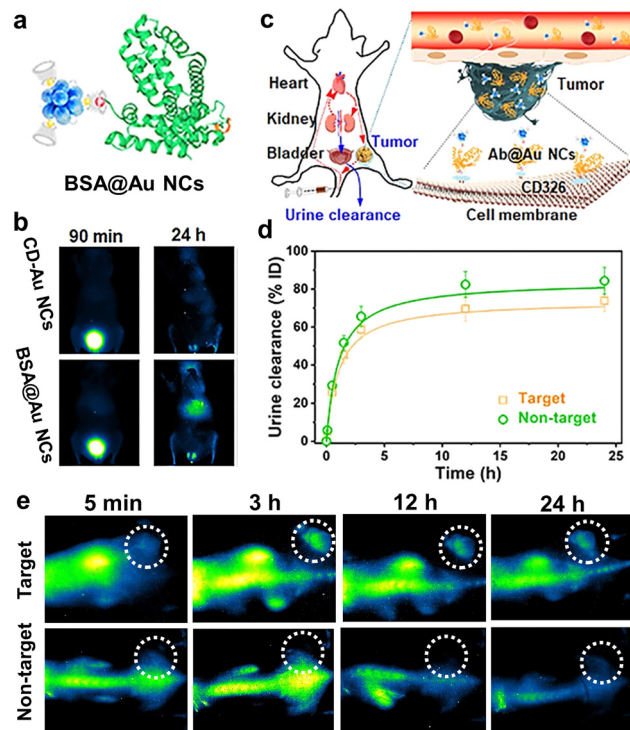


**Fig. 14** (a) Sketch map of the BSA@Au NCs *via* host-guest interaction. (b) Representative PL images of mice after the injection of CD-Au NCs and BSA@Au NCs. (c) Schematic of renal-clearable antibody-modified Au NCs for tumor targeting. (d) Urine clearance properties and (e) PL images of mice after injection of antibody@Au NCs (target) and CD-Au NCs (non-target), respectively. Adapted with permission.<sup>125</sup> Copyright 2021, Wiley-VCH.

Haase *et al.* reported the efficient photo upconversion in colloidal lanthanide-doped  $\text{NaYF}_4$  nanocrystals.<sup>243</sup> The development of the core-shell structure and co-doping design further improves the upconversion luminescence QYs of lanthanide-doped nanocrystals.<sup>244-247</sup> Significantly, owing to the weakened light scattering and absorption of tissues in the NIR-II regions, lanthanide NPs with NIR-II emissions have currently attracted increasing attention in PL bioimaging. The fantastic upconversion NIR-I PL and down-shifting NIR-II PL upon deep-tissue penetrable light excitation (*e.g.*, 808, 980, 1208 nm, and X-ray sources) make lanthanide nanoprobe a unique multifunctional imaging tool *in vivo*.<sup>248,249</sup>

Notably, high-quality lanthanide NPs are generally prepared in organic solvents with surface coating of oleic acid (and/or oleylamine) ligands. It is nowadays a routine to control the nanocrystal size and morphology of lanthanide-doped NPs.<sup>252-254</sup> To engineer functional nanoprobe, much efforts have been devoted to conducting surface modifications through silica and polymer coating and surface ligand exchange strategies.<sup>255,256</sup> The rich surface lanthanide ions facilitate facile polymer functionalization *via* both electrostatic interaction and the strong coordination between  $\text{Ln}^{3+}$  and carboxyl and amino groups. In comparison with nanoprobe established based on QDs and metal NCs, lanthanide nanoprobe might show advantages in the well-tunable and narrow PL in NIR-I/II regions and the



multiple excitation lights (e.g., NIR lasers and X-rays), which promise broad bioimaging application. However, ultrasmall lanthanide NPs may encounter low luminescence QYs, owing to small absorption cross-section and surface quenching. In 2010, Prasad *et al.* prepared ultrasmall (7.1 nm, hard size) NaYbF<sub>4</sub>:2% Tm<sup>3+</sup> NPs with high upconversion efficiency than that of classical NaYF<sub>4</sub>:20% Yb<sup>3+</sup>, 2% Tm<sup>3+</sup> NPs.<sup>257</sup> So far, several strategies have been proposed to increase PL efficiency in ultrasmall lanthanide NPs, such as host engineering and energy transfer modulation.<sup>257–263</sup> Interestingly, Liu *et al.* discovered that the UV emissions of ultrasmall (5 nm, hard size) NaGdF<sub>4</sub>:Yb/Tm NPs can be boosted by about 11 000 folds after coordinating surface ions with bidentate molecules (namely pyridine-2-carboxylic acid), which may induce reconstruction of the orbital hybridization and crystal-field splitting of surface Yb<sup>3+</sup>.<sup>264</sup> In spite of these attempts, studies on highly luminescent ultrasmall lanthanide-doped NPs are still in infancy.<sup>265</sup>

With regard to toxicity, many studies have been carried out to examine the *in vitro* and *in vivo* toxicity of lanthanide NPs, most of which have indicated their low toxicity to cells and animals.<sup>266</sup> However, time- and concentration-dependent cytotoxicity was observed in several reports.<sup>267</sup> It is also required to consider the nephrotoxicity of Gd<sup>3+</sup> and other lanthanide ions. Besides, bare lanthanide NPs were reported to induce serious cytotoxicity due likely to strong interactions with biological molecules such as adenosine triphosphate (ATP).<sup>268,269</sup> Nevertheless, lanthanide NPs have shown relatively low *in vitro* and *in vivo* toxicity after suitable functionalization (e.g., peptides, proteins, phospholipid shell).<sup>270,271</sup>

**4.3.2 *In vivo* biodistribution and body clearance.** Owing to the relatively low toxicity and high photo- and chemical-stability, lanthanide NPs are regarded as biocompatible probes.<sup>266,272</sup> Different from the hard size below 10 nm of QDs and metal NCs, lanthanide NPs often have sizes between 20 nm and 100 nm to achieve high PL QYs. Lanthanide NPs within such a size range tend to be accumulated in the RES after intravenous injection. In 2010, Li and colleagues studied the *in vivo* long-term biodistribution of Ln<sup>3+</sup>-doped NaYF<sub>4</sub> NPs (11.5 nm, hard size), showing initial accumulation in the liver and spleen after intravenous injection and gradual body clearance over 115 days (Fig. 15).<sup>250</sup> Such behaviors were similar to those of silica coated NaYF<sub>4</sub> NPs with observable body clearance after 7 days.<sup>273</sup> However, Liu and coworkers observed the long-term body retention (over 3 months) of 30 nm (hard size) NaYF<sub>4</sub>:Ln NPs coated with polyacrylic acid (PAA) and PEG layers.<sup>274</sup> The surface chemistry, particle size, and administration manner therefore can greatly affect the biodistribution and clearance of lanthanide nanoprobes.<sup>266</sup>

In the past decade, the excretion pathway of lanthanide NPs has been increasingly researched. For example, Li and coworkers utilized radioisotope labeling to track the biodistribution of lanthanide NPs (hard size, ~22 nm), revealing high accumulation in the mononuclear phagocyte systems. Only a fraction of lanthanide NPs were excreted into mice feces (<5%) *via* the hepatic clearance pathway.<sup>275</sup> When decreasing particle sizes or changing surface properties, it is feasible to elevate the

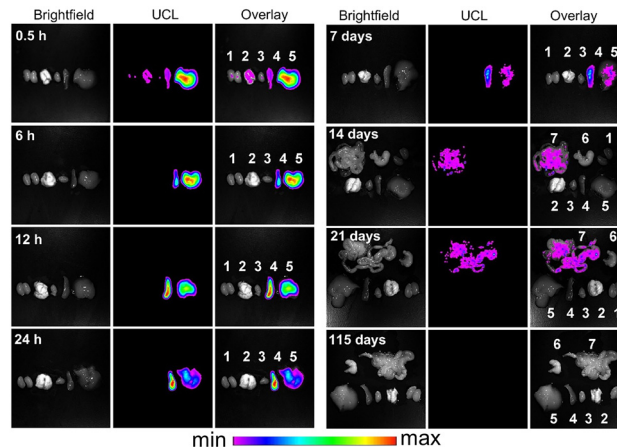


Fig. 15 Real-time *ex vivo* upconversion PL imaging of mice with the intravenous injection of PAA-lanthanide NPs. Sites 1, 2, 3, 4, 5, 6, and 7 indicate the kidney, lungs, heart, spleen, liver, stomach, and intestine regions, respectively. Adapted with permission.<sup>250</sup> Copyright 2010, Elsevier.

hepatic clearance efficiency of NPs.<sup>276</sup> For instance, Dai *et al.* reported the surface functionalization of lanthanide NPs with cross-linked hydrophilic polymers, resulting in a notably enhanced hepatic clearance efficiency of ~90% (Fig. 16).<sup>251</sup> Notably, sub-6 nm lanthanide NPs have also been prepared for PL imaging. Zhang's group reported that lanthanide NPs of 5.3 nm HD size can be excreted into both feces (~45%) and urine (~30%) at the fourth day post intravenous injection.<sup>122</sup> Prasad and colleagues studied the *in vivo* clearance efficiency of Ln<sup>3+</sup>-doped NaGdF<sub>4</sub> NPs with a HD diameter of ~5.1 nm. The injected NPs were almost eliminated from the body, showing a liver clearance of 55% and a kidney clearance of 40% over 4 days.<sup>277</sup> Overall, ultrasmall lanthanide NPs may be favorable to

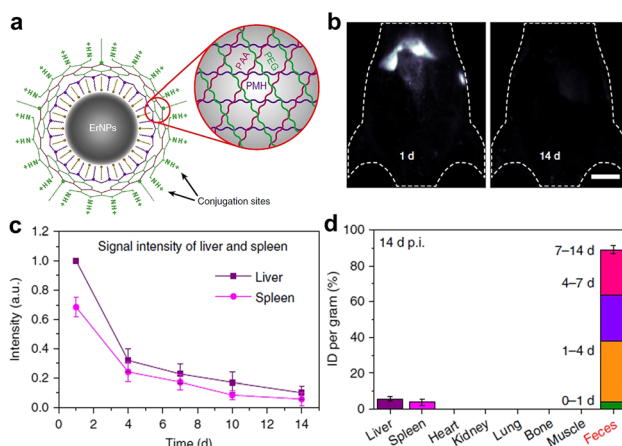


Fig. 16 (a) Sketch map of cross-linking polymer modified hydrophilic lanthanide NPs. (b) PL imaging of mice at 1 d and 14 d post injection of Er<sup>3+</sup>-doped lanthanide NPs. (c) PL intensity in the liver and spleen post injection. (d) Organ and tissue accumulation at 14 d post injection. The excreted amount of lanthanide NPs in the faeces within different time periods is also shown. Adapted with permission.<sup>251</sup> Copyright 2019, Springer Nature.



be excreted *via* both liver and kidney pathways, while large-sized lanthanide NPs tend to accumulate in the body for a relatively long time. Nevertheless, lanthanide nanoprobe are body-clearable, which can be beneficial for long-term *in vivo* PL bioimaging.

**4.3.3 *In vivo* PL bioimaging.** To construct ultrasmall lanthanide nanoprobe for PL bioimaging, the synthesis of sub-10 nm lanthanide NPs with bright PL is the first essential challenge. Previous studies have realized it by changing the synthetic methodologies, such as the design of ion doping and core-shell structure, which has been reviewed.<sup>260,265,278</sup> In 2011, Li *et al.* reported the synthesis of ultrasmall NaLuF<sub>4</sub>:Gd/Yb/Tm NPs (HD size, 8.6 nm) with intense upconversion PL, realizing cell labeling and *in vivo* sensitive upconversion PL tracking.<sup>279</sup> Ultrasmall upconversion nanoprobe can also be adopted for multimodal tumor imaging.<sup>280,281</sup> In spite of these advances, the upconversion PL efficiency of lanthanide NPs is still far less than that of down-shifting PL. Moreover, NIR-II PL imaging with low background signals and high tissue penetration depth has led to increasing research interest in NIR-II-emitting lanthanide nanoprobe. For example, Zhang *et al.* synthesized 1064 nm-emitting Nd<sup>3+</sup>-doped NPs (HD size, 5.3 nm), which can be functionalized with GSH to construct ROS-activatable nanoprobe (Fig. 17).<sup>122</sup> The ultrasmall nanoprobe were trapped in inflamed areas subjected to the ROS-triggered crosslinking reaction, achieving precise NIR-II PL imaging of mice inflammation. Meanwhile, other free nanoprobe were able to be excreted into the feces and urine, leading to the high-contrast *in vivo* PL imaging.

Apart from the conventional excitation of UV-vis and NIR lights, lanthanide NPs can also emit PL upon excitation of high-energy rays, such as X-rays and cathode rays.<sup>282</sup> Because of the broad clinical use and nearly limitless tissue penetration depth of X-rays, X-ray-activated PL imaging offers a new opportunity

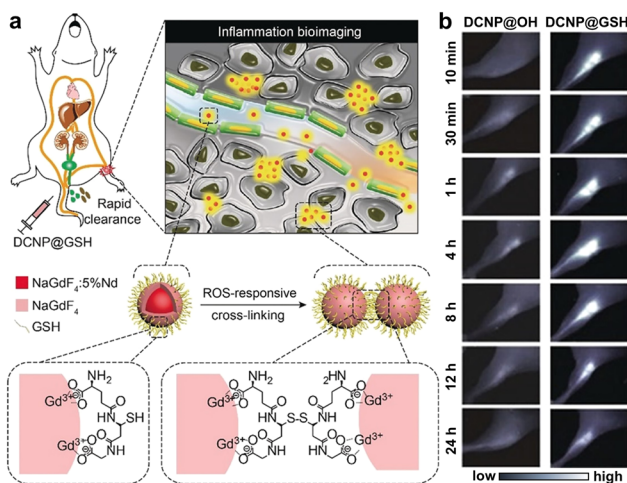


**Fig. 17** (a) Schematic illustration of the design and NIR-II PL imaging of inflammation using ultrasmall lanthanide nanoprobe. ROS responsive crosslinking of the nanoprobe is shown. (b) NIR-II PL imaging of mice inflammation after injecting different nanoprobe. Adapted with permission.<sup>122</sup> Copyright 2018, Wiley-VCH.

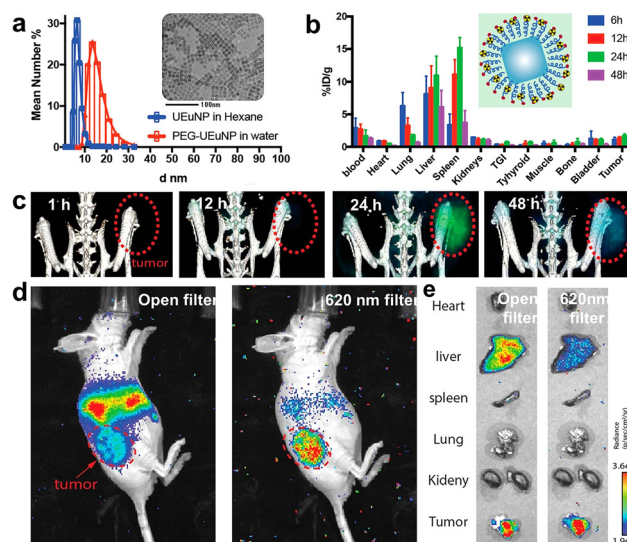


**Fig. 18** (a) HD diameters and TEM image of ultrasmall europium-doped NPs. (b) Biodistribution of PEG functionalized <sup>89</sup>Zr-europium NPs in tumor-bearing mice after intravenous injection. (c) PET imaging and (d) Cerenkov imaging of tumor-bearing mice. (e) Cerenkov imaging of *ex vivo* organs. Adapted with permission.<sup>31</sup> Copyright 2021, American Chemical Society.

for deep-tissue disease diagnosis and further clinical translation.<sup>283</sup> In 2011, Xing *et al.* synthesized small Eu<sup>3+</sup>-doped NPs with a hard size of 14 nm, and utilized their intense X-ray-excited NIR radioluminescence for *in vivo* imaging, which showed better imaging contrast than the conventional NIR imaging.<sup>284</sup> X-ray-excited NIR-II imaging was also presented through utilizing core-shell Er<sup>3+</sup>-doped lanthanide NPs, enabling sensitive *in vivo* visualization of lymph nodes.<sup>285</sup> Recently, lanthanide NPs with X-ray-excited NIR-I/II persistent radioluminescence have been studied, allowing high-contrast imaging in deep tissue.<sup>286,287</sup> In addition, it was realized to translate UV-vis Cerenkov luminescence of radioisotopes into NIR lights for *in vivo* PL imaging by combining with lanthanide NPs.<sup>288,289</sup> For example, Grimm *et al.* integrated the ultrasmall europium-doped NPs (hard size 7 nm, HD size 11 nm) with <sup>89</sup>Zr isotopes for simultaneous positron emission tomography (PET) and NIR PL imaging (Fig. 18).<sup>31</sup> The original Cerenkov radiation in the UV-vis region can excite lanthanide NPs and emit NIR PL signals to address the limited tissue penetration depth of UV-vis excitation light. Such a design provides new possibilities to improve the practical medical application of the Cerenkov radiation. However, sub-10 nm ultrasmall lanthanide NPs are still rarely explored for *in vivo* PL bioimaging currently, which might be due to their relatively low PL efficiency.

#### 4.4 Silicon nanoparticles

**4.4.1 General features.** Silicon is considered as the second most abundant element in the earth's crust after oxygen, leading to the wide applications of silicon materials in various fields, including photonics, microelectronics, and biomedicine.<sup>290-292</sup> Note that biologically used Si-based nanomaterials mainly include sub-10 nm ultrasmall silicon NPs



and non-luminescent silica NPs.<sup>293</sup> With the crystal size near bulk-Si exciton Bohr radius ( $\sim 4$  nm), ultrasmall silicon NPs possess unique optical properties (e.g., PL).<sup>294,295</sup> Luminescent silicon NPs usually have low cytotoxicity and tunable PL in the UV-vis and NIR range. Notably, silicon NPs could be biodegraded into metabolizable molecules (e.g., silicic acid) in the biological environment.<sup>296–298</sup> This makes silicon NPs very promising for clinical translation. Excitingly, ultrasmall silica NPs have been approved by the U.S. Food and Drug Administration as imaging agents for human clinical trials.<sup>26,299</sup>

In the last several years, luminescent silicon NPs have been widely utilized for *in vitro* biodetection and *in vivo* imaging.<sup>298,300,301</sup> The synthesis method can be roughly divided into two main categories, namely “top-down” and “bottom-up” approaches. The former means the crushing of large-sized silicon precursors into silicon NPs by physicochemical treatments, such as chemical etching, laser ablation, thermal decomposition, and mechanical milling.<sup>292,302,303</sup> These methods offer a facile strategy to synthesize silicon NPs with tunable emissions, but it needs hazardous agents or treatments, such as high-concentration HF and heat treatments. The alternative bottom-up methods rely on the self-assembly of molecular silicon precursors under microwave and solvent-thermal treatments.<sup>304–306</sup> This strategy can obtain silicon NPs with decided surface chemistry by using different precursors.<sup>298</sup> Significantly, the crystal size of silicon NPs markedly impacts the PL emission wavelength, lifetime, and QY, due to the PL origin from the recombination of quantum confined charge carriers of silicon.<sup>297,299</sup> Silicon NPs are prone to be oxidized and biodegraded in the biological environment,<sup>296</sup> which may reduce crystal size and affect PL properties.<sup>307,308</sup> Consequently, surface passivation of hydrogen-terminated silicon NPs is necessary for improving their photostability. It has been found that the PL and photostability of silicon NPs were improved by surface coating of organic ligands (e.g., alkene and alkyne ligands).<sup>309</sup> For example, Sato *et al.* coated silicon NPs with silicone elastomer as the passivation layer and improved their photostability in the atmosphere and in various solvents.<sup>310</sup> Typically, silicon NPs can be functionalized with polymers and other biological agents *via* hydrosilylation and functional phospholipid coating.<sup>293,311</sup>

**4.4.2 *In vivo* biodistribution and toxicity.** Biological toxicity and the *in vivo* clearance manner are the two key considerations that determine whether nanomaterials can be further used for biomedical applications. Notably, silicon NPs possess lower cytotoxicity compared to heavy metal-containing QDs.<sup>312</sup> Although silicon NPs may have ROS generation-associated toxicity at high doses in cells and animals, their good *in vivo* clearance can greatly raise long-term safety.<sup>313</sup> It has also been found that silicon NPs were degraded into silicic acid *in vivo* and excreted *via* the kidney.<sup>314–316</sup> Sailor *et al.* reported that luminescent porous silicon NPs were almost biodegraded in biological media within 4 h ( $>95\%$ ). The silicon NPs were accumulated first in the liver and spleen, and then gradually degraded within 4 weeks post injection without causing noticeable *in vivo* toxicity.<sup>314</sup> Ultrasmall silicon NPs of HD size below

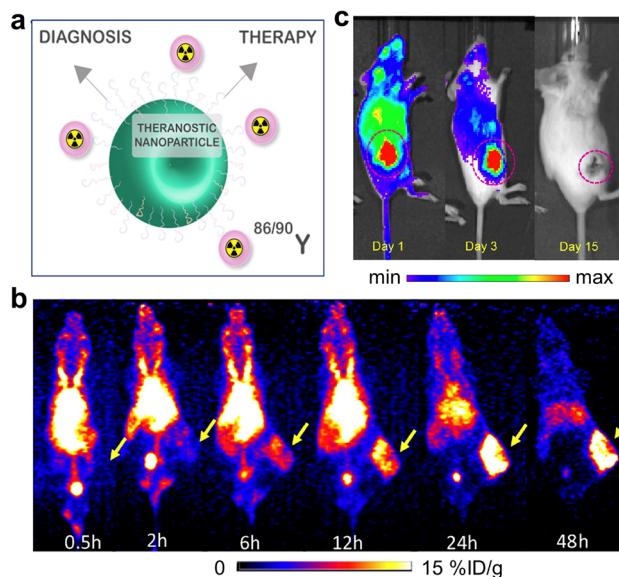


Fig. 19 (a) Sketch map of  $^{90/86}\text{Y}$ -labeled silica NPs for diagnosis and therapy applications. (b) Time evolution of PET images of tumor-bearing mice injected with  $^{90/86}\text{Y}$ -labeled silica NPs. (c) Time evolution of Cerenkov luminescence images of mice after injection. Adapted with permission.<sup>16</sup> Copyright 2021, American Chemical Society.

5 nm also allow high renal clearance and urine excretion. Louie and Kauzlarich synthesized manganese-doped silicon NPs with hard size below 5 nm and HD diameters ranging from 8 nm to 43 nm depending on the surface coatings.<sup>317</sup> These silicon NPs were nontoxic to mammalian cells, and can be labeled with the  $^{64}\text{Cu}^{2+}$  complex for biodistribution analysis *via* PET imaging. The results revealed their kidney clearance way and partial accumulation in the liver.<sup>318</sup> Recently, Cai *et al.* conjugated ultrasmall silica NPs (HD size, 13.5 nm) with the isotopic pair  $^{90/86}\text{Y}$  and systematically tracked their *in vivo* biodistribution and clearance.<sup>16</sup> It was observed that the silica NPs conferred enhanced tumor targeting and rapid hepatobiliary and renal clearance, showing high-contrast tumor imaging performance (Fig. 19).

In 2014, a first-in-human clinical trial of silica NPs was reported for tumor diagnosis (Fig. 20).<sup>26</sup> In this trial, silica NPs with HD sizes of 6–7 nm were modified with  $^{124}\text{I}$ , PEG, and peptides, thus facilitating systematic evaluation of their safety, pharmacokinetics, clearance properties, and cancer targeting efficacy *via* PET and CT imaging. The silica NPs were renal-clearable, and outperformed the clinical standard radiotracers in imaging sensitivity and specificity of human melanoma. As supported by many studies, silicon/silica NPs significantly hold high clinical translation potential.<sup>320,321</sup>

**4.4.3 *In vivo* luminescence imaging.** In order to prepare silicon nanoprobe, hydrophilic molecules and polymers are frequently employed as surface coating agents during the synthesis or during post-synthesis modification.<sup>322,323</sup> In particular, amphiphilic polymers protect silicon NPs from the oxidation and also improve their water dispersibility and *in vivo* blood circulation life.<sup>324,325</sup> Targeting agents, such as



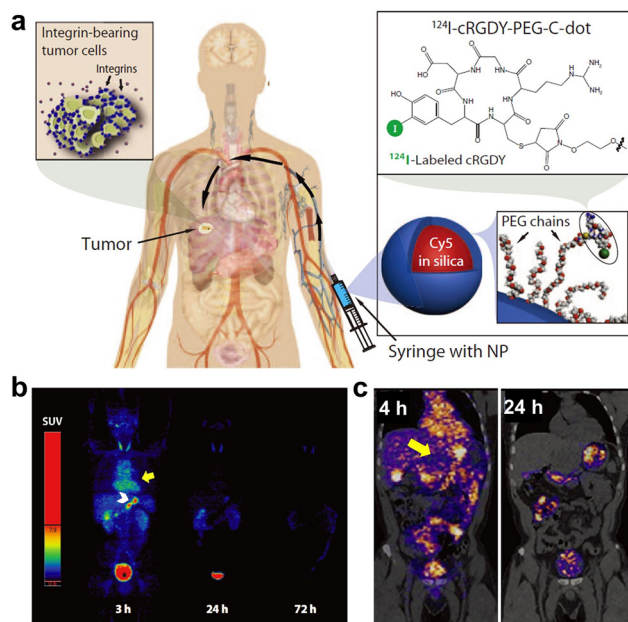


Fig. 20 (a) Schematic illustration of C dots and *in vivo* imaging. (b) Time-dependent PET imaging of human after intravenous injection of C dots (bladder, heart, and bowel are marked with \*, yellow arrow, and white arrowhead, respectively). (c) PET-CT images of human at 4 h and 24 h post injection (the tumor metastasis site is marked). Adapted with permission.<sup>26</sup> Copyright 2009, American Association for the Advancement of Science.

peptides, antibodies, and oligosaccharides, can be functionalized on silicon NPs to endow them with specific targeting capability to various diseases.<sup>326–328</sup> In 2004, Ruckenstein *et al.* reported the synthesis of NIR-emitting silicon NPs with relatively high stability for live cell imaging,<sup>329</sup> which motivated the increasing exploitation of silicon NPs for PL bioimaging.<sup>290,297,330,331</sup> Prasad *et al.* demonstrated the synthesis of PEGylated silicon NPs with intense and tunable emissions at 450–900 nm.<sup>319</sup> The PEGylation and RGD peptide modification can bypass rapid oxidative degradation and RES uptake during blood circulation, thus achieving sensitive PL imaging of sentinel lymph nodes and mouse tumors (Fig. 21). Moreover, PL in the liver and spleen almost disappeared (>95%) after 2 months, indicative of gradual *in vivo* degradation property. In another attempt, cyclic RGD-conjugated silicon NPs (hard size, ~4 nm) were designed to specifically label PAT-3 for imaging muscle attachment structures in *Caenorhabditis elegans*.<sup>328</sup> Vancomycin can then be immobilized on silicon NPs to enable *in vivo* tracking of *Staphylococcus aureus* infections for a long time (8 days),<sup>332</sup> and to rapidly image Gram-positive bacteria-induced keratitis in living mice.<sup>333</sup> Based on the strong PL of silicon NPs, He *et al.* further explored the labeling of exosomes with silicon NPs (SiNPs@EXO) for *in vivo* imaging.<sup>334</sup> Significantly, SiNPs@EXO showed high biosafety and enabled sensitive diagnosis of metastatic lymph nodes (Fig. 22). Also, NIR-II-emitting silicon NPs have been synthesized and applied to *in vivo* bioimaging. Fujii *et al.* first synthesized ~9 nm (hard size) silicon NPs with NIR-II PL centered at ~1000 nm.<sup>335</sup> They further improved NIR-II PL *via* doping boron and phosphorus,

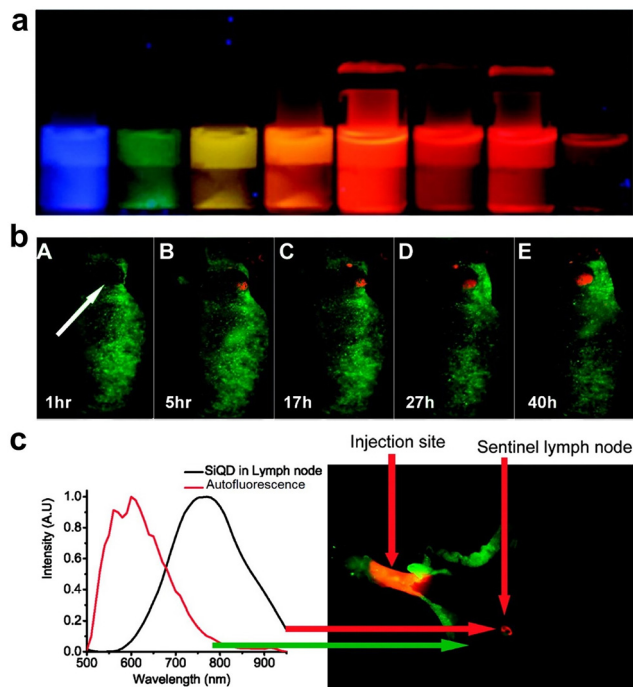


Fig. 21 (a) Photograph of emission-tunable silicon NPs upon 365 nm lamp excitation. (b) Time-dependent PL imaging of Panc-1 tumor-bearing mice after injection of RGD-modified silicon NPs. (c) Sentinel lymph node imaging upon local injection of silicon NPs. Adapted with permission.<sup>319</sup> Copyright 2011, American Chemical Society.

achieving a QY of ~1.74%.<sup>336,337</sup> Taking advantage of the microscale lifetime (>10 μs), luminescent silicon NPs can also be employed for time-gated PL imaging.<sup>338</sup>

Apart from the bioimaging by using the inherent luminescence of silicon NPs, non-luminescent silica NPs can also be explored for *in vivo* molecular PL imaging by integrating with fluorescent dyes.<sup>293,339</sup> This can be achieved by either encapsulating NIR dyes in the silica matrix or modifying them on the surface. In contrast to silicon NPs, dye-doped silica NPs may have richer structures, compositions, and morphology types (*e.g.*, pore structure, shape, dopant, *etc.*), thus allowing diverse bioapplication scenarios.<sup>340</sup> For example, Chen *et al.* developed fluorescent dye-doped ultrasmall silica NPs (~6 nm, HD size) for *in vivo* melanoma-targeted PL imaging and molecular phenotyping of sentinel lymph nodes.<sup>341</sup> The ultrasmall silica NPs were modified with Cy5.5 and CW800 dyes to construct two spectrally distinct ultrasmall nanoprobe for multiplex imaging. Therefore, the simultaneous imaging of two tumor-associated biomarkers was capable of identifying the metastatic tumors and their heterogeneity in the nodes. Such an imaging tool facilitates intraoperative imaging guided surgical decision-making and improves surgical efficacy.

In addition, it is feasible to encapsulate the lanthanide chelates and radioisotopes in silica NPs for *in vivo* PL imaging.<sup>293</sup> The long-lived luminescence of lanthanide ions offers the potential for time-resolved *in vivo* imaging.<sup>342,343</sup> Meanwhile, radioisotopes enable Cherenkov luminescence imaging for improving imaging depth and sensitivity *in vivo*.<sup>344</sup>



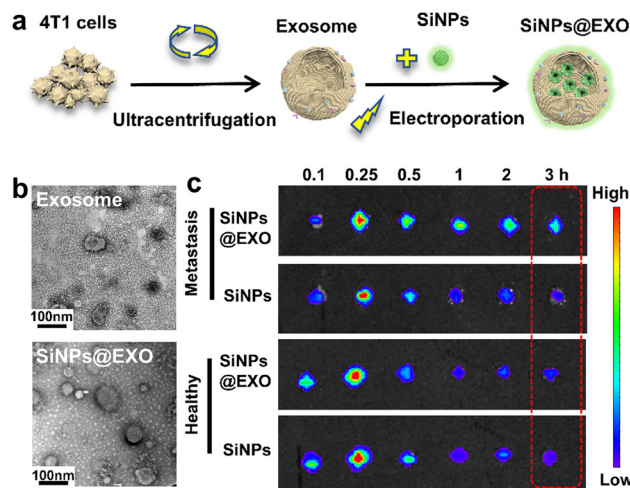


Fig. 22 (a) Schematic illustration of the preparation of the exosome and the silicon NP-labelled exosome (SiNPs@EXO). (b) TEM images of the exosome and SiNPs@EXO. (c) PL imaging of the popliteal lymph nodes in healthy mice and lymphatic metastatic mice at various times post injection. Adapted with permission.<sup>334</sup> Copyright 2021, American Chemical Society.

Silicon/silica NPs are therefore very promising nanoprobess for *in vivo* imaging of diseases, and may be clinically applicable in the near future by virtue of the ongoing clinical trial.

#### 4.5 Other ultrasmall luminescent nanoprobess

Apart from the aforementioned nanoprobess, there are several other kinds of ultrasmall luminescent nanoprobess.<sup>33,34</sup> One typical example is the renal clearable ultrasmall dye-doped nanoprobess, such as dye-doped AGuIX (activation and guiding of irradiation by X-rays) NPs, aggregation-induced emission (AIE) nanodots, and nanosized dye hybrids.<sup>345–348</sup> Besides, luminescent metal chalcogenide dots (*e.g.*, MoS<sub>2</sub>, WSe<sub>2</sub>, *etc.*), carbon dots, and polymer dots have been explored as renal clearable nanoprobess for *in vivo* bioimaging of tumors.<sup>349–352</sup> The past few years have also witnessed the size reduction of classical luminescent NPs down to the sub-10 nm region. For example, ultrasmall (2.5 nm, hard size) NPs with persistent luminescence were synthesized, enabling the satisfactory persistent luminescence and renal clearance properties for *in vivo* imaging.<sup>353,354</sup> We believe that more and more kinds of ultrasmall luminescent nanoprobess will be emerging with the rapid development in nanoscience.

## 5. Conclusions and perspectives

In this review, we have presented the pressing demand of exploiting sub-10 nm ultrasmall luminescent nanoprobess for *in vivo* imaging, and summarized recent advances of PL bioimaging based on various vital kinds of ultrasmall luminescent nanoprobess. We have discussed the size-dependent nano-bio interactions and compared the ultrasmall nanoprobess with conventional molecular fluorophores and large-sized probes. Notably, ultrasmall nanoprobess may have relatively low RES uptake and weak nonspecific accumulation in the body, thus

helping to image *in vivo* diseases of interest with high sensitivity. Recent studies have proven the significance of ultrasmall luminescent nanoprobess in molecule/protein labeling and *in vivo* tracking of kidney/bladder diseases, which usually cannot be achieved by large-sized nanoprobess. Nevertheless, it is improper to draw the conclusion that ultrasmall nanoprobess outperform large-sized nanoprobess in PL imaging *in vivo*. With the continued discovery of novel ultrasmall NPs and the design of functional nanoprobess, the sensitivity and selectivity of PL imaging could be further improved. In contrast to molecular and large-sized probes, ultrasmall luminescent nanoprobess have distinct advantages (and disadvantages) and deserve future increasing explorations and clinical trials.

Since the clinical approval of PEGylated liposomal doxorubicin (Doxil) in 1995, considerable efforts have been devoted to developing nanomaterials for cancer imaging and therapy. Hitherto, a number of imaging NPs have been clinically approved or undergoing clinical trials, as exemplified in Table 1.<sup>355,356</sup> Notably, a vast majority of the approved imaging nanoagents are implemented for magnetic resonance imaging (MRI), most probably due to the pervasive use of MRI in clinical diagnosis. Some nanoagents for ultrasound imaging are also clinically available. However, there is still a big gap between material engineering and clinical trial/translation of imaging nanoprobess. Regarding PL imaging, one example is the ultrasmall Cornell dots (7 nm, HD size) that have been in clinical trial for tumor-targeted PL imaging and positron emission tomography. Despite high imaging sensitivity and spatial resolution, PL imaging faces some challenges for its clinical applications.<sup>357</sup> A major challenge could be the limited penetration depth of PL imaging in the body. Excitingly, the emerging NIR-II imaging has extended tissue penetration depth from millimeters to centimeters. Also, further improvement in the PL QYs of nanoprobess is highly desired. Moreover, PL nanoprobess are capable of realizing surgical navigation, in which the deep tissue imaging is sometimes not necessary.<sup>358–360</sup> Additionally, it is still difficult to attain nanoprobess with clinically acceptable toxicity, biodistribution, and clearance properties. Ultrasmall nanoprobess with efficient renal clearance have garnered increasing interest in clinical trials (such as quantum dots as shown in Table 1). Besides, imaging nanoprobess intended for clinical use should be reproducible on a large scale and of high quality. In this context, atomically precise metal NCs have some advantages such as well-defined structures and compositions, which may meet some requirements for quality control of clinical agents. Though a number of imaging nanoprobess have been explored for *in vivo* PL imaging, these underutilized nanoprobess need further in-depth investigation for advancing clinical translation.

Furthermore, regarding the design of ultrasmall luminescent nanoprobess, there are still many challenges to be solved. Firstly, when particle sizes decrease to the sub-10 nm level, the absorption coefficient and PL QYs of NPs may drop sharply. For example, as for lanthanide NPs, the controlled synthesis of sub-10 nm core-shell NPs remains a challenge and their PL QYs and brightness are usually low because of the low absorption



Table 1 Examples of imaging nanoparticles (and microparticles) that have been clinically approved or are undergoing clinical trials

Name	Material composition	Identifiers	Size	Imaging mode	Diseases and applications	Approval and phase status
Feridex (Ferumoxides)	Fe <sub>3</sub> O <sub>4</sub> -γ-Fe <sub>2</sub> O <sub>3</sub> with dextran coating	NA	100 nm	MR	Imaging of liver lesions	FDA (1996) Discontinued (2008)
Resovist	Fe <sub>3</sub> O <sub>4</sub> with carboxydextran coating	NA	60 nm	MR	Imaging of liver lesions	Sweden (2001), discontinued (2009) FDA (2009)
Feraheme (Ferumoxytol)	Carbohydrate-coated ultra-small super-paramagnetic iron oxide	NA	17–31 nm	MR	Anaemia, and pancreatic cancer	FDA (2009)
Ferumoxsil	Siloxane-coated non-stoichiometric magnetite	NA	400 nm	MR	Gastrointestinal imaging	FDA (1996)
Definity	Perflutren lipid microsphere	NA	1.1–3.3 μm	US	Cardiovascular diseases, and prostatic neoplasm	FDA (2001)
Optison	Albumin coated Perflutren lipid microsphere	NA	3–4.5 μm	US	Echocardiography, and renal cell carcinoma	FDA (1997), EMA (1998)
<sup>124</sup> I-cRGDY-PEG-dots	<sup>124</sup> I-labeled cRGDY silica nanoparticle	NCT01266096	~ 7 nm	PET	Melanoma and malignant brain tumors	Startup (2011) Phase NA
Fluorescent cRGDY-PEG-Cy5.5-C dots	Silica nanoparticles, cRGDY-PEG-Cy5.5	NCT02106598	~ 8 nm	FL	Head and neck melanoma; Imaging-guided intraoperative mapping of nodal metastases	Startup (2014), phase 2 (recruiting)
<sup>64</sup> Cu-NOTA-PSMAi-PEG-Cy5.5-C' dots	Ultrasmall silica nanoparticles, <sup>64</sup> Cu-NOTA-PSMAi-PEG-Cy5.5	NCT04167969	~ 10 nm	PET/MR	Prostate cancer	Startup (2021) Phase 1 (recruiting)
QDs-VELD	CdS/ZnS QDs-COOH, veldoreotide (VELD)	NCT04138342	~ 10 nm	FL	Breast cancer, skin cancer, and skin diseases	Startup (2019) Phase 1 (recruiting)
ONM-100	Micelle conjugated to indocyanine green	NCT03735680	< 100 nm	FL	Intraoperative imaging of solid tumors	Startup (2019) Phase 2 (completed)
AGuIX	Polysiloxane Gd-chelate based nanoparticles	NCT04789486	~ 3 nm	MR	Lung tumors and pancreatic cancer	Startup (2021) Phase 2 (recruiting)

Abbreviations: MR, magnetic resonance; US, ultrasound; PET, positron emission tomography; FL, fluorescence; FDA, Food and Drug Administration; EMA, European Medicines Agency; NA, not applicable. The identifiers, phase status, and startup year information were found on ClinicalTrials.gov.

coefficient and increased defect quenching. It is highly demanded to develop new strategies for improving the PL QYs and brightness of ultrasmall NPs. Secondly, in order to satisfy the general threshold value of renal clearance, a limited number of agents are available for surface functionalization of ultrasmall nanoprobe. For instance, amphiphilic polymers, biomimetic targeting agents (*e.g.*, cell membrane), and large-sized proteins that may markedly increase HD diameters of ultrasmall nanoprobe are not suitable for surface functionalization. This hampers the design of ultrasmall luminescent nanoprobe and highlights the growing need of new functionalization strategies. Thirdly, although ultrasmall NPs can facilitate rapid renal clearance, their relatively short blood circulation time may weaken *in vivo* accumulation in the desired tumor sites. Modifying ultrasmall nanoprobe with the specific targeting ligand/antibody will be helpful. This however is still challenging, especially in imaging the orthotopic tumors located in major organs and brain. Designing size-changeable smart assemblies of ultrasmall NPs could be an alternative strategy for tumor targeting, but the clearance pathway of nanoprobe needs more investigation. Fourthly, it is also highly needed to develop commercial mature imaging apparatus to improve imaging performance in large animals. It could be interesting to develop PL imaging techniques that

can practically address the unmet needs in clinical disease imaging and therapy. Similar demands lie in establishing standardized *in vivo* imaging evaluation methods. Fifthly, the long-term *in vivo* safety of ultrasmall nanoprobe requires more in-depth studies. For example, it is hard to know whether the nanoprobe has side effects on the body after long-term metabolism and transformation.

Nevertheless, increasing studies and advances have showcased that ultrasmall luminescent nanoprobe can offer great opportunities for *in vivo* PL imaging and clinical application. With the rapid development of nanoprobe and PL imaging techniques, we strongly believe that ultrasmall luminescent nanoprobe will be a powerful engine for the development of the PL bioimaging technique, and may propel realization of precise diagnosis and therapy of diverse diseases *in vivo*.

## Author contributions

S. Li, X. Song, J. Xie, and H. Yang conceived the review, S. Li, J. Wei, Q. Yao, and X. Song drafted the manuscript, Q. Yao helped to revise the structure and content, and X. Song, J. Xie, and H. Yang supervised the project and finalized the manuscript.



## Conflicts of interest

There are no conflicts to declare.

## Acknowledgements

This work was supported by the National Natural Science Foundation of China (No. 22027805, 22274024 and 22071174), the Major Project of Science and Technology of Fujian Province (No. 2020HZ06006), the Young Elite Scientist Sponsorship Program by CAST (No. YESS20200110), and China Postdoctoral Science Foundation (No. 2022M720737, 2021T140117).

## Notes and references

- D. P. Cormode, T. Skajaa, Z. A. Fayad and W. J. Mulder, *Arterioscler., Thromb., Vasc. Biol.*, 2009, **29**, 992–1000.
- M. Schaferling, *Angew. Chem., Int. Ed.*, 2012, **51**, 3532–3554.
- K. D. Wegner and N. Hildebrandt, *Chem. Soc. Rev.*, 2015, **44**, 4792–4834.
- V. Ntziachristos, C. Bremer and R. Weissleder, *Eur. Radiol.*, 2003, **13**, 195–208.
- R. Weissleder and M. Nahrendorf, *Proc. Natl. Acad. Sci. U. S. A.*, 2015, **112**, 14424–14428.
- K. Pu, N. Chattopadhyay and J. Rao, *J. Controlled Release*, 2016, **240**, 312–322.
- H. S. Peng and D. T. Chiu, *Chem. Soc. Rev.*, 2015, **44**, 4699–4722.
- U. Resch-Genger, M. Grabolle, S. Cavaliere-Jaricot, R. Nitschke and T. Nann, *Nat. Methods*, 2008, **5**, 763–775.
- K. Zhang, Y. J. Gao, P. P. Yang, G. B. Qi, J. P. Zhang, L. Wang and H. Wang, *Adv. Healthcare Mater.*, 2018, **7**, e1800344.
- D. Kim, N. Lee, Y. I. Park and T. Hyeon, *Bioconjugate Chem.*, 2017, **28**, 115–123.
- J. Zhao, D. Zhong and S. Zhou, *J. Mater. Chem. B*, 2018, **6**, 349–365.
- W. R. Algar, M. Massey, K. Rees, R. Higgins, K. D. Krause, G. H. Darwish, W. J. Peveler, Z. Xiao, H. Y. Tsai, R. Gupta, K. Lix, M. V. Tran and H. Kim, *Chem. Rev.*, 2021, **121**, 9243–9358.
- X. He, J. Gao, S. S. Gambhir and Z. Cheng, *Trends Mol. Med.*, 2010, **16**, 574–583.
- Z. Li, Q. Sun, Y. Zhu, B. Tan, Z. P. Xu and S. X. Dou, *J. Mater. Chem. B*, 2014, **2**, 2793–2818.
- K. Zarschler, L. Rocks, N. Licciardello, L. Boselli, E. Polo, K. P. Garcia, L. De Cola, H. Stephan and K. A. Dawson, *Nanomedicine*, 2016, **12**, 1663–1701.
- C. A. Ferreira, S. Goel, E. B. Ehlerding, Z. T. Rosenkrans, D. Jiang, T. Sun, E. Aluicio-Sarduy, J. W. Engle, D. Ni and W. Cai, *Nano Lett.*, 2021, **21**, 4692–4699.
- X. Jiang, B. Du, Y. Huang and J. Zheng, *Nano Today*, 2018, **21**, 106–125.
- M. Yu and J. Zheng, *ACS Nano*, 2015, **9**, 6655–6674.
- Z. H. Hu, W. H. Chen, J. Tian and Z. Cheng, *Trends Mol. Med.*, 2020, **26**, 469–482.
- M. Yu, J. Zhou, B. Du, X. Ning, C. Authement, L. Gandee, P. Kapur, J. T. Hsieh and J. Zheng, *Angew. Chem., Int. Ed.*, 2016, **55**, 2787–2791.
- M. Yu, J. Xu and J. Zheng, *Angew. Chem., Int. Ed.*, 2019, **58**, 4112–4128.
- C. N. Loynachan, A. P. Soleimany, J. S. Dudani, Y. Lin, A. Najer, A. Bekdemir, Q. Chen, S. N. Bhatia and M. M. Stevens, *Nat. Nanotechnol.*, 2019, **14**, 883–890.
- J. G. Huang, C. Xie, X. D. Zhang, Y. Y. Jiang, J. C. Li, Q. L. Fan and K. Y. Pu, *Angew. Chem., Int. Ed.*, 2019, **58**, 15120–15127.
- L. Shang, K. Nienhaus and G. U. Nienhaus, *J. Nanobiotechnol.*, 2014, **12**, 5.
- J. Huang, J. Li, Y. Lyu, Q. Miao and K. Pu, *Nat. Mater.*, 2019, **18**, 1133–1143.
- E. Phillips, O. Penate-Medina, P. B. Zanzonico, R. D. Carvajal, P. Mohan, Y. Ye, J. Humm, M. Gonen, H. Kalaigian, H. Schoder, H. W. Strauss, S. M. Larson, U. Wiesner and M. S. Bradbury, *Sci. Transl. Med.*, 2014, **6**, 260ra149.
- D. Cassano, S. Pocovi-Martinez and V. Voliani, *Bioconjugate Chem.*, 2018, **29**, 4–16.
- W. R. Algar, K. Susumu, J. B. Delehanty and I. L. Medintz, *Anal. Chem.*, 2011, **83**, 8826–8837.
- D. Jiang, Y. Pan, H. Yao, J. Sun, W. Xiong, L. Li, F. Zheng, S. Sun and J. J. Zhu, *Anal. Chem.*, 2022, **94**, 9074–9080.
- S. M. van de Looij, E. R. Hebels, M. Viola, M. Hembury, S. Oliveira and T. Vermonden, *Bioconjugate Chem.*, 2022, **33**, 4–23.
- Q. Zhang, E. C. Pratt, R. Tamura, A. Ogirala, H. T. Hsu, N. Farahmand, S. O'Brien and J. Grimm, *Nano Lett.*, 2021, **21**, 4217–4224.
- Z. Y. Liu, A. A. Liu, H. Fu, Q. Y. Cheng, M. Y. Zhang, M. M. Pan, L. P. Liu, M. Y. Luo, B. Tang, W. Zhao, J. Kong, X. Shao and D. W. Pang, *J. Am. Chem. Soc.*, 2021, **143**, 12867–12877.
- S. Mosleh-Shirazi, M. Abbasi, M. Shafiee, S. R. Kasaei and A. M. Amani, *Mater. Today Commun.*, 2021, **26**, 102064.
- R. Q. Yin, X. C. Zhang, J. X. Ge, L. Wen, L. Chen, J. F. Zeng, Z. Li and M. Y. Gao, *Part. Part. Syst. Char.*, 2021, **38**, 2000270.
- K. Y. Zheng and J. P. Xie, *Trends Chem.*, 2020, **2**, 665–679.
- S. Behzadi, V. Serpooshan, W. Tao, M. A. Hamaly, M. Y. Alkawareek, E. C. Dreaden, D. Brown, A. M. Alkilany, O. C. Farokhzad and M. Mahmoudi, *Chem. Soc. Rev.*, 2017, **46**, 4218–4244.
- J. Mosquera, I. Garcia and L. M. Liz-Marzan, *Acc. Chem. Res.*, 2018, **51**, 2305–2313.
- X. Wang, X. Cui, Y. Zhao and C. Chen, *Sci. China: Life Sci.*, 2020, **63**, 1168–1182.
- J. J. Rennick, A. P. R. Johnston and R. G. Parton, *Nat. Nanotechnol.*, 2021, **16**, 266–276.
- M. Sousa de Almeida, E. Susnik, B. Drasler, P. Taladriz-Blanco, A. Petri-Fink and B. Rothen-Rutishauser, *Chem. Soc. Rev.*, 2021, **50**, 5397–5434.
- S. Zhang, H. Gao and G. Bao, *ACS Nano*, 2015, **9**, 8655–8671.



- 42 A. C. Marques, P. J. Costa, S. Velho and M. H. Amaral, *J. Controlled Release*, 2020, **320**, 180–200.
- 43 H. Zhu, L. Gao, X. Jiang, R. Liu, Y. Wei, Y. Wang, Y. Zhao, Z. Chai and X. Gao, *Chem. Commun.*, 2014, **50**, 3695–3698.
- 44 H. Liang, K. Yang, Y. Yang, Z. Hong, S. Li, Q. Chen, J. Li, X. Song and H. Yang, *Nano Lett.*, 2022, **22**, 9045–9053.
- 45 M. Gao, T. Yang, W. Qin, Q. Wang, M. Huang, H. Peng, M. Shao, W. Yao, X. Yi, G. Sun and X. He, *Small*, 2022, **18**, e2204689.
- 46 W. Jiang, B. Y. Kim, J. T. Rutka and W. C. Chan, *Nat. Nanotechnol.*, 2008, **3**, 145–150.
- 47 F. Lu, S. H. Wu, Y. Hung and C. Y. Mou, *Small*, 2009, **5**, 1408–1413.
- 48 H. Gao, W. Shi and L. B. Freund, *Proc. Natl. Acad. Sci. U. S. A.*, 2005, **102**, 9469–9474.
- 49 A. Albanese, P. S. Tang and W. C. Chan, *Annu. Rev. Biomed. Eng.*, 2012, **14**, 1–16.
- 50 H. Yuan, J. Li, G. Bao and S. Zhang, *Phys. Rev. Lett.*, 2010, **105**, 138101.
- 51 A. M. Smith, K. A. Johnston, S. E. Crawford, L. E. Marbella and J. E. Millstone, *Analyst*, 2016, **142**, 11–29.
- 52 A. M. Alkilany, L. Zhu, H. Weller, A. Mews, W. J. Parak, M. Barz and N. Feliu, *Adv. Drug Delivery Rev.*, 2019, **143**, 22–36.
- 53 L. Tong, E. Lu, J. Pichaandi, P. P. Cao, M. Nitz and M. A. Winnik, *Chem. Mater.*, 2015, **27**, 4899–4910.
- 54 K. Huang, H. Ma, J. Liu, S. Huo, A. Kumar, T. Wei, X. Zhang, S. Jin, Y. Gan, P. C. Wang, S. He, X. Zhang and X. J. Liang, *ACS Nano*, 2012, **6**, 4483–4493.
- 55 Y. Jiang, S. Huo, T. Mizuhara, R. Das, Y. W. Lee, S. Hou, D. F. Moyano, B. Duncan, X. J. Liang and V. M. Rotello, *ACS Nano*, 2015, **9**, 9986–9993.
- 56 M. Liang, I. C. Lin, M. R. Whittaker, R. F. Minchin, M. J. Monteiro and I. Toth, *ACS Nano*, 2010, **4**, 403–413.
- 57 E. Oh, J. B. Delehanty, K. E. Sapsford, K. Susumu, R. Goswami, J. B. Blanco-Canosa, P. E. Dawson, J. Granek, M. Shoff, Q. Zhang, P. L. Goering, A. Huston and I. L. Medintz, *ACS Nano*, 2011, **5**, 6434–6448.
- 58 N. Hoshyar, S. Gray, H. Han and G. Bao, *Nanomedicine*, 2016, **11**, 673–692.
- 59 A. C. Anselmo and S. Mitragotri, *Adv. Drug Delivery Rev.*, 2017, **108**, 51–67.
- 60 Y. Hui, X. Yi, D. Wibowo, G. Yang, A. P. J. Middelberg, H. Gao and C. X. Zhao, *Sci. Adv.*, 2020, **6**, eaaz4316.
- 61 P. Guo, D. Liu, K. Subramanyam, B. Wang, J. Yang, J. Huang, D. T. Augustine and M. A. Moses, *Nat. Commun.*, 2018, **9**, 130.
- 62 L. Gong, Y. Chen, K. He and J. Liu, *ACS Nano*, 2019, **13**, 1893–1899.
- 63 Y. Wei, N. R. Jana, S. J. Tan and J. Y. Ying, *Bioconjugate Chem.*, 2009, **20**, 1752–1758.
- 64 E. Porret, L. Sancey, A. Martin-Serrano, M. I. Montanez, R. Seeman, A. Yahia-Armar, H. Okuno, F. Gomez, A. Ariza, N. Hildebrandt, J. B. Fleury, J. L. Coll and X. Le Guevel, *Chem. Mater.*, 2017, **29**, 7497–7506.
- 65 S. Ashraf, J. Park, M. A. Bichelberger, K. Kantner, R. Hartmann, P. Maffre, A. H. Said, N. Feliu, J. Lee, D. Lee, G. U. Nienhaus, S. Kim and W. J. Parak, *Nanoscale*, 2016, **8**, 17794–17800.
- 66 X. Wang, X. Wang, X. Bai, L. Yan, T. Liu, M. Wang, Y. Song, G. Hu, Z. Gu, Q. Miao and C. Chen, *Nano Lett.*, 2019, **19**, 8–18.
- 67 P. C. Ke, S. Lin, W. J. Parak, T. P. Davis and F. Caruso, *ACS Nano*, 2017, **11**, 11773–11776.
- 68 M. Hadjidemetriou and K. Kostarelos, *Nat. Nanotechnol.*, 2017, **12**, 288–290.
- 69 M. P. Monopoli, C. Aberg, A. Salvati and K. A. Dawson, *Nat. Nanotechnol.*, 2012, **7**, 779–786.
- 70 R. Cai and C. Chen, *Adv. Mater.*, 2019, **31**, e1805740.
- 71 W. Xiao and H. Gao, *Int. J. Pharm.*, 2018, **552**, 328–339.
- 72 M. Mahmoudi, N. Bertrand, H. Zope and O. C. Farokhzad, *Nano Today*, 2016, **11**, 817–832.
- 73 S. Schottler, K. Landfester and V. Mailander, *Angew. Chem., Int. Ed.*, 2016, **55**, 8806–8815.
- 74 A. K. Barui, J. Y. Oh, B. Jana, C. Kim and J. H. Ryu, *Adv. Ther.*, 2020, **3**, 1900124.
- 75 A. Lesniak, A. Salvati, M. J. Santos-Martinez, M. W. Radomski, K. A. Dawson and C. Aberg, *J. Am. Chem. Soc.*, 2013, **135**, 1438–1444.
- 76 P. Del Pino, B. Pelaz, Q. Zhang, P. Maffre, G. U. Nienhaus and W. J. Parak, *Mater. Horiz.*, 2014, **1**, 301–313.
- 77 Q. Xiao, M. Zoulikha, M. Qiu, C. Teng, C. Lin, X. Li, M. A. Sallam, Q. Xu and W. He, *Adv. Drug Delivery Rev.*, 2022, **186**, 114356.
- 78 T. Cedervall, I. Lynch, S. Lindman, T. Berggard, E. Thulin, H. Nilsson, K. A. Dawson and S. Linse, *Proc. Natl. Acad. Sci. U. S. A.*, 2007, **104**, 2050–2055.
- 79 A. Bekdemir and F. Stellacci, *Nat. Commun.*, 2016, **7**, 13121.
- 80 J. Piella, N. G. Bastus and V. Puntès, *Bioconjugate Chem.*, 2017, **28**, 88–97.
- 81 M. M. Yin, P. Dong, W. Q. Chen, S. P. Xu, L. Y. Yang, F. L. Jiang and Y. Liu, *Langmuir*, 2017, **33**, 5108–5116.
- 82 A. Verma, O. Uzun, Y. Hu, Y. Hu, H. S. Han, N. Watson, S. Chen, D. J. Irvine and F. Stellacci, *Nat. Mater.*, 2008, **7**, 588–595.
- 83 S. D. Li and L. Huang, *Mol. Pharm.*, 2008, **5**, 496–504.
- 84 S. Chen and X. J. Liang, *Sci. China: Life Sci.*, 2018, **61**, 371–372.
- 85 S. H. Li, Y. L. Chen, W. Zhu, W. Yang, Z. W. Chen, J. B. Song, X. R. Song, X. Chen and H. H. Yang, *Adv. Funct. Mater.*, 2021, **31**, 2010337.
- 86 M. Bjornmalm, K. J. Thurecht, M. Michael, A. M. Scott and F. Caruso, *ACS Nano*, 2017, **11**, 9594–9613.
- 87 J. W. Nichols and Y. H. Bae, *J. Controlled Release*, 2014, **190**, 451–464.
- 88 D. X. Sun, S. Zhou and W. Gao, *ACS Nano*, 2020, **14**, 12281–12290.
- 89 X. Duan and Y. Li, *Small*, 2013, **9**, 1521–1532.
- 90 H. C. Fischer and W. C. Chan, *Curr. Opin. Biotechnol*, 2007, **18**, 565–571.
- 91 S. J. Soenen, P. Rivera-Gil, J. M. Montenegro, W. J. Parak, S. C. De Smedt and K. Braeckmans, *Nano Today*, 2011, **6**, 446–465.



- 92 L. Yildirim, N. T. Thanh, M. Loizidou and A. M. Seifalian, *Nano Today*, 2011, **6**, 585–607.
- 93 K. L. Aillon, Y. Xie, N. El-Gendy, C. J. Berkland and M. L. Forrest, *Adv. Drug Delivery Rev.*, 2009, **61**, 457–466.
- 94 H. Arami, A. Khandhar, D. Liggitt and K. M. Krishnan, *Chem. Soc. Rev.*, 2015, **44**, 8576–8607.
- 95 M. Ajdary, M. A. Moosavi, M. Rahmati, M. Falahati, M. Mahboubi, A. Mandegary, S. Jangjoo, R. Mohammadinejad and R. S. Varma, *Nanomaterials*, 2018, **8**, 634.
- 96 S. Y. Wang, F. Y. Li, X. Hu, M. Lv, C. H. Fan and D. S. Ling, *Adv. Ther.*, 2018, **1**, 1800059.
- 97 G. B. Yang, S. Z. F. Phua, A. K. Bindra and Y. L. Zhao, *Adv. Mater.*, 2019, **31**, 1805730.
- 98 B. Wang, X. He, Z. Zhang, Y. Zhao and W. Feng, *Acc. Chem. Res.*, 2013, **46**, 761–769.
- 99 Y. N. Zhang, W. Poon, A. J. Tavares, I. D. McGilvray and W. C. W. Chan, *J. Controlled Release*, 2016, **240**, 332–348.
- 100 S. H. Li, Q. P. Ma, C. L. Wang, K. D. Yang, Z. Z. Hong, Q. S. Chen, J. B. Song, X. R. Song and H. H. Yang, *Anal. Chem.*, 2022, **94**, 2641–2647.
- 101 B. J. Du, M. X. Yu and J. Zheng, *Nat. Rev. Mater.*, 2018, **3**, 358–374.
- 102 L. Cheng, D. Jiang, A. Kamkaew, H. F. Valdovinos, H. J. Im, L. Feng, C. G. England, S. Goel, T. E. Barnhart, Z. Liu and W. Cai, *Adv. Funct. Mater.*, 2017, **27**, 1702928.
- 103 T. Cao, Y. Yang, Y. Sun, Y. Wu, Y. Gao, W. Feng and F. Li, *Biomaterials*, 2013, **34**, 7127–7134.
- 104 X. Wang, X. Zhong, J. Li, Z. Liu and L. Cheng, *Chem. Soc. Rev.*, 2021, **50**, 8669–8742.
- 105 G. Yang, S. Z. F. Phua, A. K. Bindra and Y. Zhao, *Adv. Mater.*, 2019, **31**, e1805730.
- 106 R. Mout, D. F. Moyano, S. Rana and V. M. Rotello, *Chem. Soc. Rev.*, 2012, **41**, 2539–2544.
- 107 J. Zhang, L. Mou and X. Jiang, *Chem. Sci.*, 2020, **11**, 923–936.
- 108 X. D. Meng, F. Yang, H. F. Dong, L. Dou and X. J. Zhang, *Nano Today*, 2021, **38**, 101156.
- 109 M. Ovais, M. Guo and C. Chen, *Adv. Mater.*, 2019, **31**, e1808303.
- 110 K. Y. Zheng and J. P. Xie, *Trends Chem.*, 2020, **2**, 665–679.
- 111 R. Q. Yin, X. C. Zhang, J. X. Ge, L. Wen, L. Chen, J. F. Zeng, Z. Li and M. Y. Gao, *Part. Part. Syst. Char.*, 2021, **38**, 2000270.
- 112 X. Luo and J. Liu, *Adv. Sci.*, 2022, **9**, e2103971.
- 113 F. Chen, K. Ma, B. Madajewski, L. Zhuang, L. Zhang, K. Rickert, M. Marelli, B. Yoo, M. Z. Turker, M. Overholtzer, T. P. Quinn, M. Gonen, P. Zanzonico, A. Tiesca, M. A. Bowen, L. Norton, J. A. Subramony, U. Wiesner and M. S. Bradbury, *Nat. Commun.*, 2018, **9**, 4141.
- 114 C. Verry, S. Dufort, B. Lemasson, S. Grand, J. Pietras, I. Tropres, Y. Cremillieux, F. Lux, S. Meriaux, B. Larrat, J. Balosso, G. Le Duc, E. L. Barbier and O. Tillement, *Sci. Adv.*, 2020, **6**, eaay5279.
- 115 X. R. Song, S. H. Li, J. Dai, L. Song, G. Huang, R. Lin, J. Li, G. Liu and H. H. Yang, *Small*, 2017, **13**, 1603997.
- 116 Y. Cui, J. Yang, Q. Zhou, P. Liang, Y. Wang, X. Gao and Y. Wang, *ACS Appl. Mater. Interfaces*, 2017, **9**, 5900–5906.
- 117 W. Yang, C. Xiang, Y. Xu, S. Chen, W. Zeng, K. Liu, X. Jin, X. Zhou and B. Zhang, *Biomaterials*, 2020, **255**, 120186.
- 118 F. Chen, K. Ma, B. Madajewski, L. Zhuang, L. Zhang, K. Rickert, M. Marelli, B. Yoo, M. Z. Turker, M. Overholtzer, T. P. Quinn, M. Gonen, P. Zanzonico, A. Tiesca, M. A. Bowen, L. Norton, J. A. Subramony, U. Wiesner and M. S. Bradbury, *Nat. Commun.*, 2018, **9**, 4141.
- 119 X. Song, W. Zhu, X. Ge, R. Li, S. Li, X. Chen, J. Song, J. Xie, X. Chen and H. Yang, *Angew. Chem., Int. Ed.*, 2021, **60**, 1306–1312.
- 120 M. H. Li, Z. Luo and Y. L. Zhao, *Chem. Mater.*, 2018, **30**, 25–53.
- 121 X. D. Lai, L. S. Tan, X. L. Deng, J. B. Liu, A. Q. Li, J. Y. Liu and J. Q. Hu, *ACS Appl. Mater. Interfaces*, 2017, **9**, 5118–5127.
- 122 M. Zhao, R. Wang, B. Li, Y. Fan, Y. Wu, X. Zhu and F. Zhang, *Angew. Chem., Int. Ed.*, 2019, **58**, 2050–2054.
- 123 P. H. Cheng and K. Y. Pu, *Nat. Rev. Mater.*, 2021, **6**, 1095–1113.
- 124 J. G. Huang, Y. Y. Jiang, J. C. Li, S. S. He, J. S. Huang and K. Y. Pu, *Angew. Chem., Int. Ed.*, 2020, **59**, 4415–4420.
- 125 X. Song, W. Zhu, X. Ge, R. Li, S. Li, X. Chen, J. Song, J. Xie, X. Chen and H. Yang, *Angew. Chem., Int. Ed.*, 2021, **60**, 1306–1312.
- 126 J. Huang, X. Chen, Y. Jiang, C. Zhang, S. He, H. Wang and K. Pu, *Nat. Mater.*, 2022, **21**, 598–607.
- 127 H. S. Choi, W. Liu, P. Misra, E. Tanaka, J. P. Zimmer, B. Itty Ipe, M. G. Bawendi and J. V. Frangioni, *Nat. Biotechnol.*, 2007, **25**, 1165–1170.
- 128 M. Bruchez, Jr., M. Moronne, P. Gin, S. Weiss and A. P. Alivisatos, *Science*, 1998, **281**, 2013–2016.
- 129 X. Michalet, F. F. Pinaud, L. A. Bentolila, J. M. Tsay, S. Doose, J. J. Li, G. Sundaresan, A. M. Wu, S. S. Gambhir and S. Weiss, *Science*, 2005, **307**, 538–544.
- 130 C. B. Murray, D. J. Norris and M. G. Bawendi, *J. Am. Chem. Soc.*, 1993, **115**, 8706–8715.
- 131 A. M. Wagner, J. M. Knipe, G. Orive and N. A. Peppas, *Acta Biomater.*, 2019, **94**, 44–63.
- 132 J. Owen and L. Brus, *J. Am. Chem. Soc.*, 2017, **139**, 10939–10943.
- 133 K. J. McHugh, L. Jing, A. M. Behrens, S. Jayawardena, W. Tang, M. Gao, R. Langer and A. Jaklenec, *Adv. Mater.*, 2018, **30**, e1706356.
- 134 D. J. Norris and M. G. Bawendi, *Phys. Rev. B: Condens. Matter Mater. Phys.*, 1996, **53**, 16338–16346.
- 135 R. E. Bailey and S. Nie, *J. Am. Chem. Soc.*, 2003, **125**, 7100–7106.
- 136 M. A. Farzin and H. Abdoos, *Talanta*, 2021, **224**, 121828.
- 137 H. R. Chandan, J. D. Schiffman and R. G. Balakrishna, *Sens. Actuators, B*, 2018, **258**, 1191–1214.
- 138 G. Pereira, C. A. P. Monteiro, G. M. Albuquerque, M. I. A. Pereira, M. P. Cabrera, P. E. Cabral, G. A. L. Pereira, A. Fontes and B. S. Santos, *J. Braz. Chem. Soc.*, 2019, **30**, 2536–2560.
- 139 Y. P. Gu, R. Cui, Z. L. Zhang, Z. X. Xie and D. W. Pang, *J. Am. Chem. Soc.*, 2012, **134**, 79–82.



- 140 S. Filali, F. Pirot and P. Miossec, *Trends Biotechnol.*, 2020, **38**, 163–177.
- 141 S. Nikazar, V. S. Sivasankarapillai, A. Rahdar, S. Gasmi, P. S. Anumol and M. S. Shanavas, *Biophys. Rev.*, 2020, **12**, 703–718.
- 142 A. Hoshino, S. Hanada and K. Yamamoto, *Arch. Toxicol.*, 2011, **85**, 707–720.
- 143 H. Sun, F. Zhang, H. Wei and B. Yang, *J. Mater. Chem. B*, 2013, **1**, 6485–6494.
- 144 C. Li, F. Li, Y. Zhang, W. Zhang, X. E. Zhang and Q. Wang, *ACS Nano*, 2015, **9**, 12255–12263.
- 145 M. L. Schipper, G. Iyer, A. L. Koh, Z. Cheng, Y. Ebenstein, A. Aharoni, S. Keren, L. A. Bentolila, J. Li, J. Rao, X. Chen, U. Banin, A. M. Wu, R. Sinclair, S. Weiss and S. S. Gambhir, *Small*, 2009, **5**, 126–134.
- 146 Y. Zhang, Y. Zhang, G. Hong, W. He, K. Zhou, K. Yang, F. Li, G. Chen, Z. Liu, H. Dai and Q. Wang, *Biomaterials*, 2013, **34**, 3639–3646.
- 147 J. Bourquin, A. Milosevic, D. Hauser, R. Lehner, F. Blank, A. Petri-Fink and B. Rothen-Rutishauser, *Adv. Mater.*, 2018, **30**, e1704307.
- 148 M. Zhang, J. Yue, R. Cui, Z. Ma, H. Wan, F. Wang, S. Zhu, Y. Zhou, Y. Kuang, Y. Zhong, D. W. Pang and H. Dai, *Proc. Natl. Acad. Sci. U. S. A.*, 2018, **115**, 6590–6595.
- 149 E. Oh, R. Liu, A. Nel, K. B. Gemill, M. Bilal, Y. Cohen and I. L. Medintz, *Nat. Nanotechnol.*, 2016, **11**, 479–486.
- 150 L. Ye, K. T. Yong, L. W. Liu, I. Roy, R. Hu, J. Zhu, H. X. Cai, W. C. Law, J. W. Liu, K. Wang, J. Liu, Y. Q. Liu, Y. Z. Hu, X. H. Zhang, M. T. Swihart and P. N. Prasad, *Nat. Nanotechnol.*, 2012, **7**, 453–458.
- 151 T. S. Hauck, R. E. Anderson, H. C. Fischer, S. Newbigging and W. C. W. Chan, *Small*, 2010, **6**, 138–144.
- 152 S. Jeong, I. Song, W. Lee, Y. M. Ryu, Y. Jung, S. Y. Kim, K. Kim, S. C. Hong, S. J. Myung and S. Kim, *Nano Lett.*, 2017, **17**, 1378–1386.
- 153 T. Pons, E. Pic, N. Lequeux, E. Cassette, L. Bezdetnaya, F. Guillemin, F. Marchal and B. Dubertret, *ACS Nano*, 2010, **4**, 2531–2538.
- 154 J. C. Kays, A. M. Saeboe, R. Toufanian, D. E. Kurant and A. M. Dennis, *Nano Lett.*, 2020, **20**, 1980–1991.
- 155 C. Xia, J. D. Meeldijk, H. C. Gerritsen and C. de Mello Donega, *Chem. Mater.*, 2017, **29**, 4940–4951.
- 156 L. Li, T. J. Daou, I. Texier, T. K. C. Tran, Q. L. Nguyen and P. Reiss, *Chem. Mater.*, 2009, **21**, 2422–2429.
- 157 X. Gao, Y. Cui, R. M. Levenson, L. W. Chung and S. Nie, *Nat. Biotechnol.*, 2004, **22**, 969–976.
- 158 W. Cai and X. Chen, *Nat. Protoc.*, 2008, **3**, 89–96.
- 159 J. Y. Zhao, G. Chen, Y. P. Gu, R. Cui, Z. L. Zhang, Z. L. Yu, B. Tang, Y. F. Zhao and D. W. Pang, *J. Am. Chem. Soc.*, 2016, **138**, 1893–1903.
- 160 J. Liu, S. K. Lau, V. A. Varma, R. A. Moffitt, M. Caldwell, T. Liu, A. N. Young, J. A. Petros, A. O. Osunkoya, T. Krogstad, B. Leyland-Jones, M. D. Wang and S. Nie, *ACS Nano*, 2010, **4**, 2755–2765.
- 161 B. Liu, B. Jiang, Z. P. Zheng and T. C. Liu, *J. Lumin.*, 2019, **209**, 61–68.
- 162 Y. P. Wang, Y. F. Jiang, M. Zhang, J. Tan, J. M. Liang, H. X. Wang, Y. P. Li, H. N. He, V. C. Yang and Y. Z. Huang, *Adv. Funct. Mater.*, 2014, **24**, 5443–5453.
- 163 X. Liu, G. B. Braun, M. Qin, E. Ruoslahti and K. N. Sugahara, *Nat. Commun.*, 2017, **8**, 343.
- 164 H. Mattoussi, G. Palui and H. B. Na, *Adv. Drug Delivery Rev.*, 2012, **64**, 138–166.
- 165 D. Geissler and N. Hildebrandt, *Anal. Bioanal. Chem.*, 2016, **408**, 4475–4483.
- 166 M. K. So, C. Xu, A. M. Loening, S. S. Gambhir and J. Rao, *Nat. Biotechnol.*, 2006, **24**, 339–343.
- 167 G. Yang, W. Wang, J. Song and J. Zhang, *Nanomedicine*, 2021, **16**, 1737–1740.
- 168 X. Sun, X. Huang, J. Guo, W. Zhu, Y. Ding, G. Niu, A. Wang, D. O. Kiesewetter, Z. L. Wang, S. Sun and X. Chen, *J. Am. Chem. Soc.*, 2014, **136**, 1706–1709.
- 169 X. Xu, H. An, D. Zhang, H. Tao, Y. Dou, X. Li, J. Huang and J. Zhang, *Sci. Adv.*, 2019, **5**, eaat2953.
- 170 Q. Li, J. Zeng, Q. Miao and M. Gao, *Front. Bioeng. Biotechnol.*, 2019, **7**, 326.
- 171 A. Zebibula, N. Alifu, L. Q. Xia, C. W. Sun, X. M. Yu, D. W. Xue, L. W. Liu, G. H. Li and J. Qian, *Adv. Funct. Mater.*, 2018, **28**, 1703451.
- 172 S. S. Ling, X. H. Yang, C. Y. Li, Y. J. Zhang, H. C. Yang, G. C. Chen and Q. B. Wang, *Angew. Chem., Int. Ed.*, 2020, **59**, 7219–7223.
- 173 W. Lian, D. T. Tu, P. Hu, X. R. Song, Z. L. Gong, T. Chen, J. B. Song, Z. Chen and X. Y. Chen, *Nano Today*, 2020, **35**, 100943.
- 174 H. M. Gil, T. W. Price, K. Chelani, J. S. G. Bouillard, S. D. J. Calaminus and G. J. Stasiuk, *Iscience*, 2021, **24**, 102189.
- 175 J. J. Zhang, Y. Lin, H. Zhou, H. He, J. J. Ma, M. Y. Luo, Z. L. Zhang and D. W. Pang, *Adv. Healthcare Mater.*, 2019, **8**, 1900341.
- 176 Y. Du, B. Xu, T. Fu, M. Cai, F. Li, Y. Zhang and Q. Wang, *J. Am. Chem. Soc.*, 2010, **132**, 1470–1471.
- 177 C. Li, W. Li, H. Liu, Y. Zhang, G. Chen, Z. Li and Q. Wang, *Angew. Chem., Int. Ed.*, 2020, **59**, 247–252.
- 178 O. T. Bruns, T. S. Bischof, D. K. Harris, D. Franke, Y. X. Shi, L. Riedemann, A. Bartelt, F. B. Jaworski, J. A. Carr, C. J. Rowlands, M. W. B. Wilson, O. Chen, H. Wei, G. W. Hwang, D. M. Montana, I. Coropceanu, O. B. Achorn, J. Kloepper, J. Heeren, P. T. C. So, D. Fukumura, K. F. Jensen, R. K. Jain and M. G. Bawendi, *Nat. Biomed. Eng.*, 2017, **1**, 0056.
- 179 Y. F. Tang, F. Pei, X. M. Lu, Q. L. Fan and W. Huang, *Adv. Opt. Mater.*, 2019, **7**, 1900917.
- 180 R. Tian, H. L. Ma, S. J. Zhu, J. Lau, R. Ma, Y. J. Liu, L. S. Lin, S. Chandra, S. Wang, X. F. Zhu, H. Z. Deng, G. Niu, M. X. Zhang, A. L. Antaris, K. S. Hettie, B. Yang, Y. Y. Liang and X. Y. Chen, *Adv. Mater.*, 2020, **32**, 1907365.
- 181 R. C. Jin, *Nanoscale*, 2015, **7**, 1549–1565.
- 182 R. C. Jin, C. J. Zeng, M. Zhou and Y. X. Chen, *Chem. Rev.*, 2016, **116**, 10346–10413.
- 183 Y. Z. Lu and W. Chen, *Chem. Soc. Rev.*, 2012, **41**, 3594–3623.



- 184 I. Chakraborty and T. Pradeep, *Chem. Rev.*, 2017, **117**, 8208–8271.
- 185 L. B. Zhang and E. K. Wang, *Nano Today*, 2014, **9**, 132–157.
- 186 E. Porret, X. Le Guevel and J. L. Coll, *J. Mater. Chem. B*, 2020, **8**, 2216–2232.
- 187 X. D. Zhang, D. Wu, X. Shen, P. X. Liu, F. Y. Fan and S. J. Fan, *Biomaterials*, 2012, **33**, 4628–4638.
- 188 L. Dong, M. Li, S. Zhang, J. Li, G. Shen, Y. Tu, J. Zhu and J. Tao, *Small*, 2015, **11**, 2571–2581.
- 189 Y. Pan, S. Neuss, A. Leifert, M. Fischler, F. Wen, U. Simon, G. Schmid, W. Brandau and W. Jahnen-Dechent, *Small*, 2007, **3**, 1941–1949.
- 190 E. Porret, X. Le Guevel and J. L. Coll, *J. Mater. Chem. B*, 2020, **8**, 2216–2232.
- 191 J. J. Li, J. J. Zhu and K. Xu, *TrAC, Trends Anal. Chem.*, 2014, **58**, 90–98.
- 192 L. Shang, S. J. Dong and G. U. Nienhaus, *Nano Today*, 2011, **6**, 401–418.
- 193 X. R. Song, N. Goswami, H. H. Yang and J. P. Xie, *Analyst*, 2016, **141**, 3126–3140.
- 194 Y. Tao, M. Q. Li, J. S. Ren and X. G. Qu, *Chem. Soc. Rev.*, 2015, **44**, 8636–8663.
- 195 Y. Negishi, K. Nobusada and T. Tsukuda, *J. Am. Chem. Soc.*, 2005, **127**, 5261–5270.
- 196 Y. Shichibu, Y. Negishi, H. Tsunoyama, M. Kanehara, T. Teranishi and T. Tsukuda, *Small*, 2007, **3**, 835–839.
- 197 H. Qian, Y. Zhu and R. Jin, *ACS Nano*, 2009, **3**, 3795–3803.
- 198 H. Qian and R. Jin, *Nano Lett.*, 2009, **9**, 4083–4087.
- 199 H. Qian, M. Zhu, Z. Wu and R. Jin, *Acc. Chem. Res.*, 2012, **45**, 1470–1479.
- 200 Y. Yu, X. Chen, Q. F. Yao, Y. Yu, N. Yan and J. P. Xie, *Chem. Mater.*, 2013, **25**, 946–952.
- 201 C. Zhou, M. Long, Y. Qin, X. Sun and J. Zheng, *Angew. Chem., Int. Ed.*, 2011, **50**, 3168–3172.
- 202 Y. G. Srinivasulu, Q. F. Yao, N. Goswami and J. P. Xie, *Mater. Horiz.*, 2020, **7**, 2596–2618.
- 203 X. Kang and M. Z. Zhu, *Chem. Soc. Rev.*, 2019, **48**, 2422–2457.
- 204 S. Wang, X. Meng, A. Das, T. Li, Y. Song, T. Cao, X. Zhu, M. Zhu and R. Jin, *Angew. Chem., Int. Ed.*, 2014, **53**, 2376–2380.
- 205 K. Pyo, V. D. Thanthirige, K. Kwak, P. Pandurangan, G. Ramakrishna and D. Lee, *J. Am. Chem. Soc.*, 2015, **137**, 8244–8250.
- 206 Z. Luo, X. Yuan, Y. Yu, Q. Zhang, D. T. Leong, J. Y. Lee and J. Xie, *J. Am. Chem. Soc.*, 2012, **134**, 16662–16670.
- 207 Z. Wu, Q. Yao, O. J. H. Chai, N. Ding, W. Xu, S. Zang and J. Xie, *Angew. Chem., Int. Ed.*, 2020, **59**, 9934–9939.
- 208 A. Cantelli, G. Guidetti, J. Manzi, V. Caponetti and M. Montalti, *Eur. J. Inorg. Chem.*, 2017, 5068–5084.
- 209 C. H. Yao, C. Q. Xu, I. H. Park, M. Zhao, Z. Y. Zhu, J. Li, X. Hai, H. Y. Fang, Y. Zhang, G. Macam, J. H. Teng, L. Li, Q. H. Xu, F. C. Chuang, J. P. Lu, C. L. Su, J. Li and J. Lu, *Angew. Chem., Int. Ed.*, 2020, **59**, 8270–8276.
- 210 Z. N. Wu, Y. H. Du, J. Liu, Q. F. Yao, T. K. Chen, Y. T. Cao, H. Zhang and J. P. Xie, *Angew. Chem., Int. Ed.*, 2019, **58**, 8139–8144.
- 211 A. Yahia-Ammar, D. Sierra, F. Merola, N. Hildebrandt and X. Le Guevel, *ACS Nano*, 2016, **10**, 2591–2599.
- 212 J. Liu, M. Yu, X. Ning, C. Zhou, S. Yang and J. Zheng, *Angew. Chem., Int. Ed.*, 2013, **52**, 12572–12576.
- 213 X. Jiang, B. Du and J. Zheng, *Nat. Nanotechnol.*, 2019, **14**, 874–882.
- 214 J. Xu and L. Shang, *Chin. Chem. Lett.*, 2018, **29**, 1436–1444.
- 215 X. Q. Meng, I. Zare, X. Y. Yan and K. L. Fan, *Wiley Interdiscip. Rev.: Nanomed. Nanobiotechnol.*, 2020, **12**, e1602.
- 216 Z. J. Qiao, J. Zhang, X. Hai, Y. C. Yan, W. L. Song and S. Bi, *Biosens. Bioelectron.*, 2021, **176**, 112898.
- 217 J. Yang, T. Wang, L. N. Zhao, V. K. Rajasekhar, S. Joshi, C. Andreou, S. Pal, H. T. Hsu, H. W. Zhang, I. J. Cohen, R. M. Huang, R. C. Hendrickson, M. M. Miele, W. B. Pei, M. B. Brendel, J. H. Healey, G. Chiosis and M. F. Kircher, *Nat. Biomed. Eng.*, 2020, **4**, 686–703.
- 218 Y. Tan, K. He, B. Tang, H. Chen, Z. Zhao, C. Zhang, L. Lin and J. Liu, *ACS Nano*, 2020, **14**, 13975–13985.
- 219 E. G. Ju, Z. Liu, Y. D. Du, Y. Tao, J. S. Ren and X. G. Qu, *ACS Nano*, 2014, **8**, 6014–6023.
- 220 T. T. Chen, Y. H. Hu, Y. Cen, X. Chu and Y. Lu, *J. Am. Chem. Soc.*, 2013, **135**, 11595–11602.
- 221 H. F. Fang, H. Yu, Q. Lu, X. Fang, Q. L. Zhang, J. T. Zhang, L. L. Zhu and Q. B. Ma, *Anal. Chem.*, 2020, **92**, 12825–12832.
- 222 Y. Chen, L. B. Li, L. S. Gong, T. Y. Zhou and J. B. Liu, *Adv. Funct. Mater.*, 2019, **29**, 1806945.
- 223 J. Q. Wang and G. Liu, *Angew. Chem., Int. Ed.*, 2018, **57**, 3008–3010.
- 224 J. Xu, M. X. Yu and J. Zheng, *Angew. Chem., Int. Ed.*, 2017, **56**, 13356–13360.
- 225 Y. Chen, D. M. Montana, H. Wei, J. M. Cordero, M. Schneider, X. Le Guevel, O. Chen, O. T. Bruns and M. G. Bawendi, *Nano Lett.*, 2017, **17**, 6330–6334.
- 226 Z. Yu, B. Musnier, K. D. Wegner, M. Henry, B. Chovelon, A. Desroches-Castan, A. Fertin, U. Resch-Genger, S. Bailly, J. L. Coll, Y. Usson, V. Jossierand and X. Le Guevel, *ACS Nano*, 2020, **14**, 4973–4981.
- 227 H. Liu, G. Hong, Z. Luo, J. Chen, J. Chang, M. Gong, H. He, J. Yang, X. Yuan, L. Li, X. Mu, J. Wang, W. Mi, J. Luo, J. Xie and X. D. Zhang, *Adv. Mater.*, 2019, **31**, e1901015.
- 228 W. Wang, Y. Kong, J. Jiang, Q. Xie, Y. Huang, G. Li, D. Wu, H. Zheng, M. Gao, S. Xu, Y. Pan, W. Li, R. Ma, M. X. Wu, X. Li, H. Zuillhof, X. Cai and R. Li, *Angew. Chem., Int. Ed.*, 2020, **59**, 22431–22435.
- 229 Q. Li, C. J. t Zeman, Z. Ma, G. C. Schatz and X. W. Gu, *Small*, 2021, **17**, e2007992.
- 230 Y. Ishida, R. D. Corpuz and T. Yonezawa, *Acc. Chem. Res.*, 2017, **50**, 2986–2995.
- 231 F. Wang and X. G. Liu, *Acc. Chem. Res.*, 2014, **47**, 1378–1385.
- 232 G. Y. Chen, C. H. Yang and P. N. Prasad, *Acc. Chem. Res.*, 2013, **46**, 1474–1486.
- 233 Y. J. Yang, D. T. Tu, Y. Q. Zhang, P. Zhang and X. Y. Chen, *Science*, 2021, **24**, 102062.
- 234 H. Li, X. Wang, T. Y. Ohulchanskyy and G. Y. Chen, *Adv. Mater.*, 2021, **33**, 2000678.



- 235 J. P. Leonard, C. B. Nolan, F. Stomeo and T. Gunnlaugsson, *Top. Curr. Chem.*, 2007, **281**, 1–43.
- 236 G. F. de Sa, O. L. Malta, C. D. Donega, A. M. Simas, R. L. Longo, P. A. Santa-Cruz and E. F. da Silva, *Coordin. Chem. Rev.*, 2000, **196**, 165–195.
- 237 J. C. G. Bunzli, *Coordin. Chem. Rev.*, 2015, **293**, 19–47.
- 238 S. V. Eliseeva and J. C. Bunzli, *Chem. Soc. Rev.*, 2010, **39**, 189–227.
- 239 H. Dong, S. R. Du, X. Y. Zheng, G. M. Lyu, L. D. Sun, L. D. Li, P. Z. Zhang, C. Zhang and C. H. Yan, *Chem. Rev.*, 2015, **115**, 10725–10815.
- 240 X. R. Song, S. H. Li, H. H. Guo, W. W. You, X. Y. Shang, R. F. Li, D. T. Tu, W. Zheng, Z. Chen, H. H. Yang and X. Y. Chen, *Angew. Chem., Int. Ed.*, 2019, **58**, 18981–18986.
- 241 Q. Q. Ma, J. Wang, Z. H. Li, X. B. Lv, L. Liang and Q. Yuan, *Small*, 2019, **15**, 1804969.
- 242 H. H. Guo, X. R. Song, W. Lei, C. He, W. W. You, Q. Z. Lin, S. Y. Zhou, X. Y. Chen and Z. Chen, *Angew. Chem., Int. Ed.*, 2019, **58**, 12195–12199.
- 243 S. Heer, K. Kompe, H. U. Gudel and M. Haase, *Adv. Mater.*, 2004, **16**, 2102–2105.
- 244 Y. Fan, L. Liu and F. Zhang, *Nano Today*, 2019, **25**, 68–84.
- 245 H. Dong, L. D. Sun, L. D. Li, R. Si, R. Liu and C. H. Yan, *J. Am. Chem. Soc.*, 2017, **139**, 18492–18495.
- 246 F. Wang, R. R. Deng, J. Wang, Q. X. Wang, Y. Han, H. M. Zhu, X. Y. Chen and X. G. Liu, *Nat. Mater.*, 2011, **10**, 968–973.
- 247 K. A. Abel, J. C. Boyer and F. C. van Veggel, *J. Am. Chem. Soc.*, 2009, **131**, 14644–14645.
- 248 S. H. Yu, D. T. Tu, W. Lian, J. Xu and X. Y. Chen, *Sci. China: Mater.*, 2019, **62**, 1071–1086.
- 249 S. W. Ding, L. F. Lu, Y. Fan and F. Zhang, *J. Rare Earth.*, 2020, **38**, 451–463.
- 250 L. Xiong, T. Yang, Y. Yang, C. Xu and F. Li, *Biomaterials*, 2010, **31**, 7078–7085.
- 251 Y. T. Zhong, Z. R. Ma, F. F. Wang, X. Wang, Y. J. Yang, Y. L. Liu, X. Zhao, J. C. Li, H. T. Du, M. X. Zhang, Q. H. Cui, S. J. Zhu, Q. C. Sun, H. Wan, Y. Tian, Q. Liu, W. Z. Wang, K. C. Garcia and H. J. Dai, *Nat. Biotechnol.*, 2019, **37**, 1322–1331.
- 252 Y. S. Liu, D. T. Tu, H. M. Zhu and X. Y. Chen, *Chem. Soc. Rev.*, 2013, **42**, 6924–6958.
- 253 G. F. Wang, Q. Peng and Y. D. Li, *Acc. Chem. Res.*, 2011, **44**, 322–332.
- 254 B. Liu, C. X. Li, P. P. Yang, Z. Y. Hou and J. Lin, *Adv. Mater.*, 2017, **29**, 1605434.
- 255 A. Sedlmeier and H. H. Gorris, *Chem. Soc. Rev.*, 2015, **44**, 1526–1560.
- 256 L. N. Sun, R. Y. Wei, J. Feng and H. J. Zhang, *Coord. Chem. Rev.*, 2018, **364**, 10–32.
- 257 G. Chen, T. Y. Ohulchanskyy, R. Kumar, H. Agren and P. N. Prasad, *ACS Nano*, 2010, **4**, 3163–3168.
- 258 S. Y. Han, R. R. Deng, X. J. Xie and X. G. Liu, *Angew. Chem., Int. Ed.*, 2014, **53**, 11702–11715.
- 259 X. D. Wang, R. R. Valiev, T. Y. Ohulchanskyy, H. Agren, C. H. Yang and G. Y. Chen, *Chem. Soc. Rev.*, 2017, **46**, 4150–4167.
- 260 C. Li, L. Xu, Z. Liu, Z. Li, Z. Quan, A. A. Al Kheraif and J. Lin, *Dalton Trans.*, 2018, **47**, 8538–8556.
- 261 D. J. Gargas, E. M. Chan, A. D. Ostrowski, S. Aloni, M. V. P. Altoe, E. S. Barnard, B. Sanii, J. J. Urban, D. J. Milliron, B. E. Cohen and P. J. Schuck, *Nat. Nanotechnol.*, 2014, **9**, 300–305.
- 262 M. Quintanilla, F. Q. Ren, D. L. Ma and F. Vetrone, *ACS Photonics*, 2014, **1**, 662–669.
- 263 Y. Zhang, Z. Z. Yu, J. Q. Li, Y. X. Ao, J. W. Xue, Z. P. Zeng, X. L. Yang and T. T. Y. Tan, *ACS Nano*, 2017, **11**, 2846–2857.
- 264 H. Xu, S. Y. Han, R. R. Deng, Q. Q. Su, Y. Wei, Y. A. Tang, X. Qin and X. G. Liu, *Nat. Photonics*, 2021, **15**, 732–737.
- 265 T. Joshi, C. Mamat and H. Stephan, *ChemistryOpen*, 2020, **9**, 703–712.
- 266 Y. Sun, W. Feng, P. Yang, C. Huang and F. Li, *Chem. Soc. Rev.*, 2015, **44**, 1509–1525.
- 267 A. Gnach, T. Lipinski, A. Bednarkiewicz, J. Rybka and J. A. Capobianco, *Chem. Soc. Rev.*, 2015, **44**, 1561–1584.
- 268 J. Tian, X. Zeng, X. Xie, S. Han, O. W. Liew, Y. T. Chen, L. Wang and X. Liu, *J. Am. Chem. Soc.*, 2015, **137**, 6550–6558.
- 269 S. Z. Chen, C. M. Zhang, G. Jia, J. L. Duan, S. X. Wang and J. C. Zhang, *Mater. Sci. Eng., C*, 2014, **43**, 330–342.
- 270 Q. Zhang, S. O'Brien and J. Grimm, *Nanotheranostics*, 2022, **6**, 184–194.
- 271 A. A. A. Ansari, A. K. K. Parchur and G. Y. Chen, *Coordin. Chem. Rev.*, 2022, **457**, 214423.
- 272 A. Gnach, T. Lipinski, A. Bednarkiewicz, J. Rybka and J. A. Capobianco, *Chem. Soc. Rev.*, 2015, **44**, 1561–1584.
- 273 R. Abdul Jalil and Y. Zhang, *Biomaterials*, 2008, **29**, 4122–4128.
- 274 L. Cheng, K. Yang, M. Shao, X. Lu and Z. Liu, *Nanomedicine*, 2011, **6**, 1327–1340.
- 275 Y. Sun, Q. Liu, J. Peng, W. Feng, Y. Zhang, P. Yang and F. Li, *Biomaterials*, 2013, **34**, 2289–2295.
- 276 H. Li, X. Wang, X. L. Li, S. J. Zeng and G. Y. Chen, *Chem. Mater.*, 2020, **32**, 3365–3375.
- 277 J. A. Damasco, T. Y. Ohulchanskyy, S. Mahajan, G. Chen, A. Singh, H. L. Kutscher, H. Huang, S. G. Turowski, J. A. Sperryak, A. K. Singh, J. F. Lovell, M. Seshadri and P. N. Prasad, *Cancer Nanotechnol.*, 2021, **12**, 4.
- 278 L. D. Sun, Y. F. Wang and C. H. Yan, *Acc. Chem. Res.*, 2014, **47**, 1001–1009.
- 279 Q. Liu, Y. Sun, T. Yang, W. Feng, C. Li and F. Li, *J. Am. Chem. Soc.*, 2011, **133**, 17122–17125.
- 280 D. Yang, Y. Dai, J. Liu, Y. Zhou, Y. Chen, C. Li, P. Ma and J. Lin, *Biomaterials*, 2014, **35**, 2011–2023.
- 281 F. Ren, L. Ding, H. Liu, Q. Huang, H. Zhang, L. Zhang, J. Zeng, Q. Sun, Z. Li and M. Gao, *Biomaterials*, 2018, **175**, 30–43.
- 282 X. Ou, X. Qin, B. Huang, J. Zan, Q. Wu, Z. Hong, L. Xie, H. Bian, Z. Yi, X. Chen, Y. Wu, X. Song, J. Li, Q. Chen, H. Yang and X. Liu, *Nature*, 2021, **590**, 410–415.
- 283 H. Y. Liang, Z. Z. Hong, S. H. Li, X. R. Song, D. Zhang, Q. S. Chen, J. Li and H. H. Yang, *Adv. Funct. Mater.*, 2021, **31**, 2006353.



- 284 C. Sun, G. Prax, C. M. Carpenter, H. Liu, Z. Cheng, S. S. Gambhir and L. Xing, *Adv. Mater.*, 2011, **23**, H195–H199.
- 285 D. J. Naczynski, C. Sun, S. Turkan, C. Jenkins, A. L. Koh, D. Ikeda, G. Prax and L. Xing, *Nano Lett.*, 2015, **15**, 96–102.
- 286 P. Pei, Y. Chen, C. Sun, Y. Fan, Y. Yang, X. Liu, L. Lu, M. Zhao, H. Zhang, D. Zhao, X. Liu and F. Zhang, *Nat. Nanotechnol.*, 2021, **16**, 1011–1018.
- 287 Z. Xue, X. Li, Y. Li, M. Jiang, H. Liu, S. Zeng and J. Hao, *ACS Appl. Mater. Interfaces*, 2017, **9**, 22132–22142.
- 288 Z. Hu, Y. Qu, K. Wang, X. Zhang, J. Zha, T. Song, C. Bao, H. Liu, Z. Wang, J. Wang, Z. Liu, H. Liu and J. Tian, *Nat. Commun.*, 2015, **6**, 7560.
- 289 S. Goel, F. Chen, E. B. Ehlerding and W. Cai, *Small*, 2014, **10**, 3825–3830.
- 290 F. Peng, Y. Su, Y. Zhong, C. Fan, S. T. Lee and Y. He, *Acc. Chem. Res.*, 2014, **47**, 612–623.
- 291 Y. He, C. H. Fan and S. T. Lee, *Nano Today*, 2010, **5**, 282–295.
- 292 J. H. Liang, C. B. Huang and X. Gong, *ACS Sustainable Chem. Eng.*, 2019, **7**, 18213–18227.
- 293 D. S. Karaman, M. P. Sarparanta, J. M. Rosenholm and A. J. Airaksinen, *Adv. Mater.*, 2018, **30**, e1703651.
- 294 S. Morozova, M. Alikina, A. Vinogradov and M. Pagliaro, *Front. Chem.*, 2020, **8**, 191.
- 295 S. Chinnathambi, S. Chen, S. Ganesan and N. Hanagata, *Adv. Healthcare Mater.*, 2014, **3**, 10–29.
- 296 M. Qiu, A. Singh, D. Wang, J. L. Qu, M. Swihart, H. Zhang and P. N. Prasad, *Nano Today*, 2019, **25**, 135–155.
- 297 B. F. McVey and R. D. Tilley, *Acc. Chem. Res.*, 2014, **47**, 3045–3051.
- 298 X. Y. Cheng, S. B. Lowe, P. J. Reece and J. J. Gooding, *Chem. Soc. Rev.*, 2014, **43**, 2680–2700.
- 299 B. Song and Y. He, *Nano Today*, 2019, **26**, 149–163.
- 300 X. Cheng, E. Hinde, D. M. Owen, S. B. Lowe, P. J. Reece, K. Gaus and J. J. Gooding, *Adv. Mater.*, 2015, **27**, 6144–6150.
- 301 X. Ji, F. Peng, Y. Zhong, Y. Su, X. Jiang, C. Song, L. Yang, B. Chu, S. T. Lee and Y. He, *Adv. Mater.*, 2015, **27**, 1029–1034.
- 302 A. S. Heintz, M. J. Fink and B. S. Mitchell, *Adv. Mater.*, 2007, **19**, 3984–3988.
- 303 Z. Yuan, T. Nakamura, S. Adachi and K. Matsuishi, *J. Phys. Chem. C*, 2017, **121**, 8623–8629.
- 304 Y. Han, Y. Chen, J. Feng, J. Liu, S. Ma and X. Chen, *Anal. Chem.*, 2017, **89**, 3001–3008.
- 305 H. L. Ye, S. J. Cai, S. Li, X. W. He, W. Y. Li, Y. H. Li and Y. K. Zhang, *Anal. Chem.*, 2016, **88**, 11631–11638.
- 306 S. Guruvenket, J. M. Hoey, K. J. Anderson, M. T. Frohlich, R. Krishnan, J. Sivaguru, M. P. Sibi and P. Boudjouk, *J. Mater. Chem. C*, 2016, **4**, 8206–8213.
- 307 A. Gupta, M. T. Swihart and H. Wiggers, *Adv. Funct. Mater.*, 2009, **19**, 696–703.
- 308 C. M. Hessel, E. J. Henderson and J. G. C. Veinot, *Chem. Mater.*, 2006, **18**, 6139–6146.
- 309 X. Li, Y. He and M. T. Swihart, *Langmuir*, 2004, **20**, 4720–4727.
- 310 K. Sato, N. Fukata, K. Hirakuri, M. Murakami, T. Shimizu and Y. Yamauchi, *Chem. – Asian J.*, 2010, **5**, 50–55.
- 311 S. Chinnathambi, S. Chen, S. Ganesan and N. Hanagata, *Adv. Healthcare Mater.*, 2014, **3**, 10–29.
- 312 M. Montalti, A. Cantelli and G. Battistelli, *Chem. Soc. Rev.*, 2015, **44**, 4853–4921.
- 313 J. Liu, F. Erogbogbo, K. T. Yong, L. Ye, J. Liu, R. Hu, H. Chen, Y. Hu, Y. Yang, J. Yang, I. Roy, N. A. Karker, M. T. Swihart and P. N. Prasad, *ACS Nano*, 2013, **7**, 7303–7310.
- 314 J. H. Park, L. Gu, G. von Maltzahn, E. Ruoslahti, S. N. Bhatia and M. J. Sailor, *Nat. Mater.*, 2009, **8**, 331–336.
- 315 L. Gu, D. J. Hall, Z. Qin, E. Anglin, J. Joo, D. J. Mooney, S. B. Howell and M. J. Sailor, *Nat. Commun.*, 2013, **4**, 2326.
- 316 H. Wang and Y. He, *Sensors*, 2017, **17**, 268.
- 317 C. Tu, X. Ma, P. Pantazis, S. M. Kauzlarich and A. Y. Louie, *J. Am. Chem. Soc.*, 2010, **132**, 2016–2023.
- 318 C. Tu, X. Ma, A. House, S. M. Kauzlarich and A. Y. Louie, *ACS Med. Chem. Lett.*, 2011, **2**, 285–288.
- 319 F. Erogbogbo, K. T. Yong, I. Roy, R. Hu, W. C. Law, W. Zhao, H. Ding, F. Wu, R. Kumar, M. T. Swihart and P. N. Prasad, *ACS Nano*, 2011, **5**, 413–423.
- 320 J. G. Croissant, K. S. Butler, J. I. Zink and C. J. Brinker, *Nat. Rev. Mater.*, 2020, **5**, 886–909.
- 321 T. I. Janjua, Y. X. Cao, C. Z. Yu and A. Papat, *Nat. Rev. Mater.*, 2021, **6**, 1072–1074.
- 322 S. Sato and M. T. Swihart, *Chem. Mater.*, 2006, **18**, 4083–4088.
- 323 Y. Y. Su, X. Y. Ji and Y. He, *Adv. Mater.*, 2016, **28**, 10567–10574.
- 324 F. Erogbogbo, K. T. Yong, I. Roy, G. X. Xu, P. N. Prasad and M. T. Swihart, *ACS Nano*, 2008, **2**, 873–878.
- 325 F. Erogbogbo, K. T. Yong, R. Hu, W. C. Law, H. Ding, C. W. Chang, P. N. Prasad and M. T. Swihart, *ACS Nano*, 2010, **4**, 5131–5138.
- 326 C. H. Lai, J. Hutter, C. W. Hsu, H. Tanaka, S. Varela-Aramburu, L. De Cola, B. Lepenies and P. H. Seeberger, *Nano Lett.*, 2016, **16**, 807–811.
- 327 C. Song, Y. Zhong, X. Jiang, F. Peng, Y. Lu, X. Ji, Y. Su and Y. He, *Anal. Chem.*, 2015, **87**, 6718–6723.
- 328 Y. F. Zhou, Y. Zhang, Y. L. Zhong, R. Fu, S. C. Wu, Q. Wang, H. Y. Wang, Y. Y. Su, H. M. Zhang and Y. He, *Nano Res.*, 2018, **11**, 2336–2346.
- 329 Z. F. Li and E. Ruckenstein, *Nano Lett.*, 2004, **4**, 1463–1467.
- 330 J. H. Warner, A. Hoshino, K. Yamamoto and R. D. Tilley, *Angew. Chem., Int. Ed.*, 2005, **44**, 4550–4554.
- 331 S. Chinnathambi, S. Chen, S. Ganesan and N. Hanagata, *Adv. Healthcare Mater.*, 2014, **3**, 10–29.
- 332 X. Zhai, B. Song, B. B. Chu, Y. Y. Su, H. Y. Wang and Y. He, *Nano Res.*, 2018, **11**, 6417–6427.
- 333 L. Zhang, X. Y. Ji, Y. Y. Su, X. Zhai, H. Xu, B. Song, A. R. Jiang, D. X. Guo and Y. He, *Nano Res.*, 2021, **14**, 52–58.
- 334 J. Han, L. Zhang, M. Cui, Y. Su and Y. He, *Anal. Chem.*, 2021, **93**, 10122–10131.



- 335 S. Takeoka, M. Fujii and S. Hayashi, *Phys. Rev. B: Condens. Matter Mater. Phys.*, 2000, **62**, 16820–16825.
- 336 M. Sakiyama, H. Sugimoto and M. Fujii, *Nanoscale*, 2018, **10**, 13902–13907.
- 337 H. Sugimoto, M. Fujii, K. Imakita, S. Hayashi and K. Akamatsu, *J. Phys. Chem. C*, 2013, **117**, 11850–11857.
- 338 Y. Xu, P. Li, D. Cheng, C. Wu, Q. Lu, W. Yang, X. Zhu, P. Yin, M. Liu, H. Li and Y. Zhang, *J. Mater. Chem. B*, 2020, **8**, 10290–10308.
- 339 K. Ma, H. Sai and U. Wiesner, *J. Am. Chem. Soc.*, 2012, **134**, 13180–13183.
- 340 R. Narayan, U. Y. Nayak, A. M. Raichur and S. Garg, *Pharmaceutics*, 2018, **10**, 118.
- 341 F. Chen, B. Madajewski, K. Ma, D. K. Zononi, H. Stambuk, M. Z. Turker, S. Monette, L. Zhang, B. Yoo, P. M. Chen, R. J. C. Meester, S. de Jonge, P. Montero, E. Phillips, T. P. Quinn, M. Gonen, S. Sequeira, E. de Stanchina, P. Zanzonico, U. Wiesner, S. G. Patel and M. S. Bradbury, *Sci. Adv.*, 2019, **5**, eaax5208.
- 342 H. Ma, B. Song, Y. Wang, D. Cong, Y. Jiang and J. Yuan, *Chem. Sci.*, 2017, **8**, 150–159.
- 343 P. Kalluru, R. Vankayala, C. S. Chiang and K. C. Hwang, *Adv. Funct. Mater.*, 2016, **26**, 7908–7920.
- 344 D. L. J. Thorek, A. Ogirala, B. J. Beattie and J. Grimm, *Nat. Med.*, 2013, **19**, 1345–1350.
- 345 F. Lux, V. L. Tran, E. Thomas, S. Dufort, F. Rossetti, M. Martini, C. Truillet, T. Doussineau, G. Bort, F. Denat, F. Boschetti, G. Angelovski, A. Detappe, Y. Cremillieux, N. Mignet, B. T. Doan, B. Larrat, S. Meriaux, E. Barbier, S. Roux, P. Fries, A. Muller, M. C. Abadjian, C. Anderson, E. Canet-Soulas, P. Bouziotis, M. Barberi-Heyob, C. Frochot, C. Verry, J. Balosso, M. Evans, J. Sidi-Boumedine, M. Janier, K. Butterworth, S. McMahon, K. Prise, M. T. Aloy, D. Ardail, C. Rodriguez-Lafresse, E. Porcel, S. Lacombe, R. Berbeco, A. Allouch, J. L. Perfettini, C. Chargari, E. Deutsch, G. Le Duc and O. Tillement, *Br. J. Radiol.*, 2019, **92**, 20180365.
- 346 D. Yan, T. Li, Y. Yang, N. Niu, D. Wang, J. Ge, L. Wang, R. Zhang, D. Wang and B. Z. Tang, *Adv. Mater.*, 2022, **34**, e2206643.
- 347 J. Xu, T. Han, Y. Wang, F. Zhang, M. Li, L. Bai, X. Wang, B. Sun, X. Wang, J. Du, K. Liu, J. Zhang and S. Zhu, *Nano Lett.*, 2022, **22**, 7965–7975.
- 348 L. Cheng, D. Jiang, A. Kamkaew, H. F. Valdovinos, H. J. Im, L. Feng, C. G. England, S. Goel, T. E. Barnhart, Z. Liu and W. Cai, *Adv. Funct. Mater.*, 2017, **27**, 2100549.
- 349 B. S. Tian, S. K. Liu, L. L. Feng, S. H. Liu, S. L. Gai, Y. L. Dai, L. S. Xie, B. Liu, P. P. Yang and Y. L. Zhao, *Adv. Funct. Mater.*, 2021, **31**, 2100549.
- 350 H. X. Liu, J. Y. Wang, Y. Q. Jing, J. Yang, X. T. Bai, X. Y. Mu, F. J. Xu, X. H. Xue, L. F. Liu, Y. M. Sun, Q. Liu, H. T. Dai, C. L. Liu and X. D. Zhang, *Part. Part. Syst. Char.*, 2017, **34**, 1700035.
- 351 S. H. Zheng, M. Zhang, H. Y. Bai, M. J. He, L. N. Dong, L. L. Cai, M. M. Zhao, Q. Wang, K. Xu and J. J. Li, *Int. J. Nanomed.*, 2019, **14**, 9513–9524.
- 352 X. Men, X. R. Geng, Z. Zhang, H. B. Chen, M. Du, Z. Y. Chen, G. Liu, C. F. Wu and Z. Yuan, *Mater. Today Bio.*, 2022, **16**, 100383.
- 353 J. Wang, Q. Z. Li, H. Zhao, W. T. Yue, K. W. Zhang, X. Y. Jiang and K. Li, *ACS Nano*, 2022, **16**, 462–472.
- 354 J. Liu, T. Lecuyer, J. Seguin, N. Mignet, D. Scherman, B. Viana and C. Richard, *Adv. Drug Delivery Rev.*, 2019, **138**, 193–210.
- 355 A. C. Anselmo and S. Mitragotri, *Bioeng. Transl. Med.*, 2019, **4**, e10143.
- 356 Imaging nanoparticle-all studies, <https://clinicaltrials.gov/ct2/results?recrs=&cond=&term=%22imaging%22+AND+%22nanoparticle%22&cntry=&state=&city=&dist=>, (accessed July 27, 2022).
- 357 S. M. Park, A. Aalipour, O. Vermesh, J. H. Yu and S. S. Gambhir, *Nat. Rev. Mater.*, 2017, **2**, 1–20.
- 358 C. Wang, W. Fan, Z. Zhang, Y. Wen, L. Xiong and X. Chen, *Adv. Mater.*, 2019, **31**, e1904329.
- 359 M. T. Olson, Q. P. Ly and A. M. Mohs, *Mol. Imaging Biol.*, 2019, **21**, 200–218.
- 360 L. J. Lauwerends, P. van Driel, R. J. Baatenburg de Jong, J. A. U. Hardillo, S. Koljenovic, G. Puppels, L. Mezzanotte, C. Lowik, E. L. Rosenthal, A. L. Vahrmeijer and S. Keereweer, *Lancet Oncol.*, 2021, **22**, e186–e195.

